

DELFT UNIVERSITY OF TECHNOLOGY
OFFSHORE & DREDGING ENGINEERING
BOTTOM-FOUNDED OFFSHORE STRUCTURES, ARCTIC & WIND

MASTER OF SCIENCE THESIS
**DEFINITION AND RESPONSE VALIDATION OF A
SIMPLIFIED AERO-SERVO-ELASTIC WIND
TURBINE MODEL**

Joost van den Bosch



Thesis committee

Committee chairman: Prof. Andrei V. Metrikine
Daily supervisor: Pim van der Male, MSc.
Committee member: Karel N. van Dalen, PhD.

Definition and Response Validation of a Simplified Aero-Servo-Elastic Wind Turbine Model

Joost van den Bosch

ABSTRACT

Currently, the foundation design of offshore wind turbines is based on a simple cantilever beam model with a mass representing the rotor and nacelle, or by making use of wind turbine simulation software such as Bladed, which is built for rotor design. The simple models are unrealistic since the dynamic interaction between the aerodynamic loads, hydrodynamic loads, control system and the structure is not included which leads to a lack of understanding of the behavior of the structure and possibly a poor design. The simulation software models, on the other hand, require input that the wind turbine designing party is not willing to provide, are computationally expensive, and since these are 'black box' models, give no insight into the system. In between these methods, there is currently unoccupied room for a hybrid model which includes relatively advanced rotor aerodynamics but remains computationally inexpensive while providing good insight into the behavior of the system.

This thesis aims to define such a model based on modification of models present in literature and validate it by comparing its behavior to commercial wind turbine design software. First, a model of only the rotor with a rigid frictionless drivetrain shaft and blade pitch control system (the model restricts itself to the above rated regime) is considered and validated by comparison with Bladed. The blades of the rotor are assumed to be identical and rigid, the flow is assumed to be attached and the wind velocity field is uniform and has only one directional component. The effect of the use of different wake models is tested and it is concluded that for a step wind input the equilibrium wake model is most suited, while for a turbulent wind input the dynamic wake model is the best option. Simplification of the model results in the conclusion that the lift and drag coefficients can be evaluated for the mean wind velocity and chosen to be time independent without having any significant effect, while the induction factor cannot be chosen to be time independent without it significantly affecting the behavior of the model. The aerodynamic torque is linearized with respect to wind velocity, rotational rotor velocity, pitch angle and induction factor, which results in an acceptable approximation while the operating conditions are within reasonable proximity of the chosen mean operation state. Afterwards, a tower structure and flexible drivetrain shaft are added to the model, which again is validated by using Bladed. Frequency domain analysis shows that the tower motions of both the model and Bladed are similar, thus validating the model. The aerodynamic excitation is linearized with respect to wind velocity, structural motion, rotational rotor velocity, pitch angle and induction factor and applied to the model including a tower structure and flexible drivetrain shaft. Finally, it is concluded that after simplification of the model and linearization of the aerodynamic excitation the model results in a good approximation of the wind turbine simulation software.

CONTENTS

Abstract	ii
1 Introduction	1
2 Theoretical framework and system definition	3
2.1 Axis system	3
2.2 Lift and drag coefficients	4
2.3 PI Blade Pitch Controller	4
2.4 Drivetrain models	5
2.4.1 One-mass or lumped model	5
2.4.2 Two-mass model	6
2.5 Induction factor	7
2.5.1 Frozen wake model	7
2.5.2 Equilibrium wake model	8
2.5.3 Dynamic wake model	9
2.6 Reference wind turbine and support structure	9
2.7 Wind signals	10
2.8 Assumptions and limitations	11
3 Rigid drivetrain model with nonlinear aerodynamic torque	13
3.1 Model description	13
3.1.1 Aerodynamic torque and thrust force	13
3.1.2 Lift and drag coefficients	14
3.2 Validation	15
3.2.1 Numerical model	15
3.2.2 Aerodynamic torque components for different operational states	15
3.2.3 Step wind input signal	16
3.2.4 Turbulent wind input signal	17
3.2.5 Low angle of attack assumption	17
3.3 Model simplification	18
3.3.1 Constant lift and drag coefficients	18
3.3.2 Frozen wake model	18

4	Rigid drivetrain model with linearized aerodynamic torque	25
4.1	Linearized approximation of the aerodynamic torque	25
4.1.1	Aerodynamic torque sensitivity to wind speed variations	26
4.1.2	Aerodynamic torque sensitivity to rotational velocity variations	27
4.1.3	Aerodynamic torque sensitivity to pitch angle variations	27
4.1.4	Aerodynamic torque sensitivity to induction variations	28
4.2	Numerical model	28
4.3	Comparison	29
4.3.1	Step wind input signal	29
4.3.2	Turbulent wind input signal	29
5	Wind turbine model with nonlinear aerodynamic excitation	33
5.1	Equation of motion	33
5.2	Numerical model	35
5.3	Validation	35
5.3.1	Step wind input signal	35
5.3.2	Turbulent wind input signal	36
6	Wind turbine model with linearized aerodynamic excitation	41
6.1	Mean aerodynamic excitation	42
6.2	Aerodynamic excitation sensitivities	42
6.2.1	Aerodynamic excitation sensitivity to wind speed variations	42
6.2.2	Aerodynamic excitation sensitivity to structural rotation	43
6.2.3	Aerodynamic excitation sensitivity to structural velocity	44
6.2.4	Aerodynamic excitation sensitivity to structural acceleration	46
6.2.5	Aerodynamic excitation sensitivity to rotational velocity variations	46
6.2.6	Aerodynamic excitation sensitivity to pitch angle variations	47
6.2.7	Aerodynamic excitation sensitivity to induction factor variations	47
6.3	Numerical model	48
6.4	Comparison	49
7	Conclusions and recommendations	53
A	NREL 5-MW Reference Wind Turbine	57
A.1	Blade properties	57
A.2	Lift and drag coefficients	57

LIST OF FIGURES

2.1	Definition of the axis system [10].	3
2.2	Schematic overview of the pitch control system.	5
2.3	One-mass drivetrain model.	6
2.4	Two-mass drivetrain model.	6
2.5	Annulus of the rotor swept area.	7
2.6	Definition of the inflow angle and angle of attack [10].	8
2.7	The different sections of the blade.	9
2.8	The step (a) and turbulent (b) wind signals used to generate results.	11
3.1	The different components of the aerodynamic torque for operational states throughout the above rated regime.	16
3.2	The highest occurring angle of attack during the turbulent wind signal at the center of each blade section, with the corresponding airfoils.	17
3.3	The lift coefficient for varying angle of attack of the different airfoils.	18
3.4	Results for step wind input with wind signal (a), rotational velocity (b), pitch angle (c), aerodynamic torque (d) and thrust force (e).	20
3.5	Results for turbulent wind input with wind signal (a), rotational velocity (b), pitch angle (c), aerodynamic torque (d) and thrust force (e).	21
3.6	Results for step wind input with wind signal (a), rotational velocity (b), pitch angle (d) for time varying coefficients and constant coefficients and rotational velocity (c) and pitch angle (e) for the dynamic wake model and frozen wake model.	22
3.7	Results for turbulent wind input with wind signal (a), rotational velocity (b), pitch angle (d) for time varying coefficients and constant coefficients and rotational velocity (c) and pitch angle (e) for the dynamic wake model and frozen wake model.	23
4.1	The aerodynamic torque sensitivity to wind speed (a), rotational velocity (b), pitch angle (c), induction factor (d) and all (e).	30
4.2	Results for step wind input with wind signal (a), rotational velocity (b), pitch angle (c), torque (d) and thrust force (e) for both the nonlinear and linearized model.	31
4.3	Results for turbulent wind input with wind signal (a), rotational velocity (b), pitch angle (c), torque (d) and thrust force (e) for both the nonlinear and linearized model.	32
5.1	Results for step wind input with wind signal (a), fore-aft motion $u_Y^1(t)$ (b), rotational velocity (c), pitch angle (d), aerodynamic torque (e) and thrust force (f) for both the nonlinear model and Bladed.	37

5.2	Results for turbulent wind input with wind signal (a), rotational velocity (b), pitch angle (c), aerodynamic torque (d) and thrust force (e) for both the nonlinear model and Bladed.	38
5.3	Side-to-side displacement of the tower top $u_X^1(t)$ (a), fore-aft motion of the tower top $u_Y^1(t)$ (b), the side-to-side motion of the tower top in the frequency domain (c) and the fore-aft displacement in the frequency domain (d).	39
6.1	Results for turbulent wind input with wind signal (a), rotational velocity (b), pitch angle (c), aerodynamic torque (d) and thrust force (e) for both nonlinear and linearized aerodynamic excitation.	50
6.2	Side-to-side displacement of the tower top $u_X^1(t)$ (a), fore-aft motion of the tower top $u_Y^1(t)$ (b), the side-to-side motion in the frequency domain (c) and the fore-aft displacement in the frequency domain (d).	51

LIST OF TABLES

2.1	General specifications of the rotor and drivetrain [7].	10
2.2	The operational parameters in the above rated regime [7].	10
A.1	The blade specifications [7].	57
A.2	The cambered lift coefficients C_L^c of the sections [7].	58
A.3	The angle of attack dependent lift coefficients C_L^α of the sections for different wind velocities in the above rated regime [7].	58
A.4	The drag coefficients (C_D) of the sections for different wind velocities in the above rated regime [7].	59
A.5	Equilibrium pitch angles for different wind velocities in the above rated regime provided by Bladed.	59

1 | INTRODUCTION

Society's dependence on fossil fuels needs to be drastically decreased in the coming years and other sustainable sources of energy need to be utilized. Offshore wind energy is one of the solutions, which is extensively applied in Europe and other places around the globe. Offshore wind energy prices are dropping, wind turbine and offshore wind farm sizes are increasing, and with over 12 GW installed offshore capacity in Europe, another 25 GW is consented [5]. The future of offshore wind energy seems to be glorious, but increasing turbine and wind farm size present new challenges and difficulties and designs should be optimized further to decrease costs even more.

Currently, the foundation design of offshore wind turbines is based on a simple cantilever beam model with a mass representing the rotor and nacelle, or by making use of wind turbine simulation software such as Bladed, which is built for rotor design. More advanced methods such as vortex panels and computational fluid dynamics are available, but not used in practice yet. The simple models are unrealistic since the dynamic interaction between the aerodynamic loads, hydrodynamic loads, control system and the structure is not included which leads to a lack of understanding of the behavior of the structure and possibly a poor design. The simulation software models, on the other hand, require input that the wind turbine designing party is not willing to provide, are computationally expensive, and since these are 'black box' models, give no insight into the system. In between these methods, there is currently unoccupied room for a hybrid model which includes rotor aerodynamics but remains computationally inexpensive while providing good insight into the behavior of the system.

A nonlinear aerodynamic rotor model for a rotor defining relations between the aerodynamic forces and the tower response and equations of motions of the turbine is presented by van der Male et al. in [10]. The paper also describes a linearization of the aerodynamic excitation with respect to the tower top motions and the wind velocity (not with respect to the rotational rotor velocity, pitch angle and induction factor), however, does not include an active pitch control system or flexible drivetrain shaft in the model and lacks a description of possible wake models that could be used. Three of the wake models available in literature, the frozen wake model, the equilibrium wake model and the dynamic wake model, are presented in [2] and [1]. A rotor and drivetrain model with a flexible shaft is presented by Zhang et al. [11], in which the reduction of lateral tower vibrations by active generator torque is investigated. This article lacks a description of the aerodynamic forces acting on the rotor. Jonkman et al. describe the blade pitch PI-controller and generator torque controller in [7] in which the software FAST is used and which also lacks an aerodynamic force description. Papers by Hwas and Katebi [6] and by Hansen et al. [4] give an in-depth description of the gain optimization and scheduling of the PI blade pitch controller, which is necessary when optimizing the control system, but this optimization falls outside the scope of this thesis. All these sources describe different components of an aero-servo-elastic wind turbine model, and are used in the definition of the model.

The goal of this thesis is to answer the question how a full model of a(n) (offshore) wind turbine which includes accurate aerodynamic rotor forces, an active pitch control system and a flexible drivetrain shaft that provides similar results as commercial software tools but with a drastic decrease in computational time and increase in insight can be defined. Secondly, what is the effect of simplifications of the model on its prediction accuracy?

The effect of the use of the different wake models and the effect of eliminating the wind velocity dependency of the lift and drag coefficients of the rotor on the behavior of the model is investigated. The final simplification looked into is the linearization of the aerodynamic forces with respect to structural motions, wind speed, rotational velocity, pitch angle and induction factor. The results generated will answer the question whether the use of a linearized aerodynamic excitation is a reasonable simplification or not.

First, a model of the rotor and drivetrain with a rigid shaft is defined by using the nonlinear aerodynamic force expressions based on attached flow provided in [10] and a reference wind turbine [7] to validate the model by comparing its output (aerodynamic forces, structural motions, rotational rotor velocity and pitch angle) to results generated with the commercial wind turbine simulation tool Bladed. The blades of the rotor are assumed to be identical and rigid, the wind is assumed to be uniform and to only have one directional component. Secondly, the effect of the use of different wake models and making the lift and drag coefficients time independent on the results is investigated. The aerodynamic torque acting on the model is linearized with respect to the wind velocity, rotational velocity of the rotor, pitch angle and induction factor, and the behavior is compared that of the model with a nonlinear aerodynamic excitation. After this, a model including a monopile support structure [3] and flexible drivetrain shaft is presented and validated with the use of Bladed, after which the effects of linearization of the aerodynamic forces in this model are looked into. The structural motions of the tower top are presented in both the time and frequency domain to make comparisons between Bladed, the model with nonlinear aerodynamic excitation, and the model with linearized aerodynamic excitation. Finally, it is concluded whether the model gives satisfying results compared to Bladed, what causes possible deviations and what can be done to improve it.

2 | THEORETICAL FRAMEWORK AND SYSTEM DEFINITION

This chapter provides theory and definitions used in the subsequent chapters, as well as a specifications of the wind turbine used to generate results. Only the most general specifications of the reference turbine will be stated in this chapter, for more specific information, the reader is referred to Appendix A. Three different wake models used to determine the induction factor are presented, besides two different ways of modeling the drivetrain of the wind turbine (the one and two-mass-model), all of which are used in the aero-servo-elastic wind turbine models defined in subsequent chapters.

2.1 AXIS SYSTEM

The axis system of the model is defined as visualized in Figure 2.1. The direction of all forces and moments acting on the tower top, which coincide with the origin of the axis system, are denoted by a subscript of the particular axis. The Y-axis coincides with the rotational axis of the rotor and the Z-axis is directed upwards, the origin is defined as the center of rotation of the tower top, r_j is the length along blade j starting from the hub. The rotational velocity of the rotor is denoted by $\Omega_R(t)$.

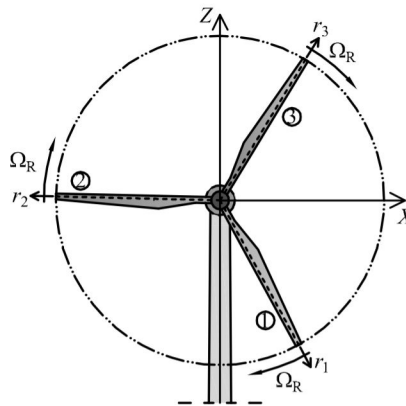


Figure 2.1: Definition of the axis system [10].

2.2 LIFT AND DRAG COEFFICIENTS

The lift and drag coefficients are dimensionless coefficients that describe the relation between the shape of an airfoil and the magnitude of the lift and drag forces generated by its presence in a flow. The coefficients vary per airfoil, are dependent on the angle of attack and the values are determined experimentally. In [10] the lift coefficient is split up into two parts. One part depends on the camber (asymmetry) of the airfoils, due to which lift is generated for an angle of attack of zero, $C_L^c(r)$. The other part is dependent on the angle of attack, $\alpha(r)$, of the relative wind flow. The relation is presented in Equation 2.1:

$$C_L(r) = C_L^c(r) + \sin(\alpha(r)) \cdot C_L^\alpha(r). \quad (2.1)$$

This approximation is only valid for low angles of attack.

2.3 PI BLADE PITCH CONTROLLER

The pitch angle of the blades is controlled by a PI-controller which contains a proportional (P) and an integral (I) term. In the above rated regime, the aim of the controller is to keep the power output of the wind turbine, $P(t)$, as close to the rated desired power output as possible to not overload the gearbox and generator. To achieve this, the rotational velocity of the high speed generator shaft, $\Omega_G(t)$, should be kept as close as possible to its rated rotational velocity, $\bar{\Omega}_G$. The deviation of the high speed shaft's rotational velocity at the generator side from its rated value, defined as $\Delta\Omega_G(t)$, is the error to which the controller responds.

$$\Omega_G(t) = \bar{\Omega}_G + \Delta\Omega_G(t) \quad (2.2)$$

Equation 2.3 describes the produced power (neglecting the efficiency of the generator) as a mean component and a time varying part, which consists of the deviation from the rated rotational velocity of the generator times the electromagnetic generator torque. Mean or rated variables are indicated by a bar, and are not dependent on time. Note that the generator torque is constant in the above rated regime.

$$P(t) = \bar{P}(t) + \Delta\Omega_G(t) \cdot T_G \quad (2.3)$$

The principle of the control system is visualized in Figure 2.2. For example, an increase in wind speed changes the aerodynamic torque acting on the rotor ($T_{R:A;Y}(t)$), consequently, an increase in torque disturbs the equilibrium which results in an acceleration and increase in rotational velocity of the low speed shaft, $\Delta\Omega_R(t)$. The low speed shaft is connected to the high speed generator shaft via the gearbox, and thus the speed of the high speed shaft, $\Delta\Omega_G(t)$, will increase as well. The high speed shaft's rotational velocity is measured and compared to a reference value ($\bar{\Omega}_G$) for the above rated regime, the differences between these two values is the 'error' which is the input of the PI-controller. The actuator generates a certain pitch angle response ($\Delta\beta(t)$) to this error which will bring the torque acting on the rotor and therefore the rotational speed of the shafts down, resulting in bringing the power output back to the rated value. The PI-controller equation for this system is described by Equation 2.4:

$$\Delta\beta(t) = K_P \Delta\Omega_G(t) + K_I \int_0^t \Delta\Omega_G(t) dt, \quad (2.4)$$

where the K_P and K_I represent the proportional and integral gain, respectively. Note that for rigid drivetrain shafts the high speed shaft's rotational velocity deviation $\Delta\Omega_G(t)$ can be replaced by $N_{GB} \Delta\Omega_R(t)$, where N_{GB} is the gearbox ratio between the low and high speed shaft of the drivetrain and $\Delta\Omega_R(t)$ is the deviation of the rotor's rotational velocity from its rated value, because every acceleration of the rotor will be immediately

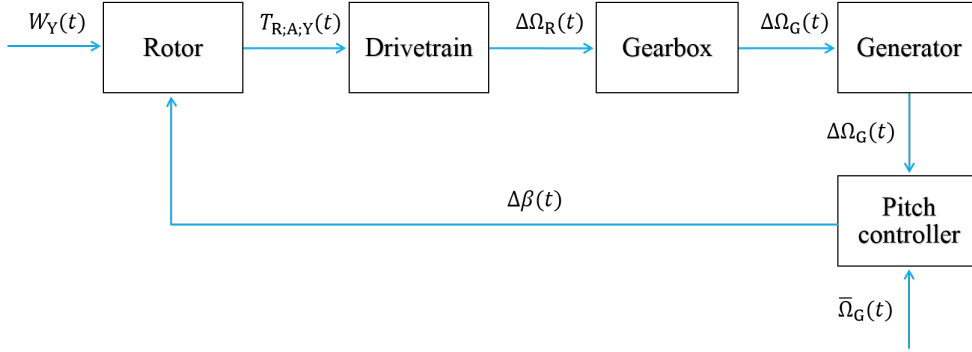


Figure 2.2: Schematic overview of the pitch control system.

followed by the generator and vice versa. This thesis does not include optimization of the control system and the models presented assume constant gains, thus no gain-scheduling is applied. The dynamics of the pitch control system are not included in any of models.

2.4 DRIVETRAIN MODELS

Although more advanced drivetrain models are present in literature [9], including the inertia of parts of the gearbox such as the gears, the drivetrain models this thesis is restricted to are the one-mass or lumped model and the two-mass model. The drivetrain of a wind turbine consist of a low speed shaft, to which the rotor is connected, and a high speed shaft, to which the generator is connected. Both shafts are connected by a gearbox, which results in the shafts having different rotational velocities and different torques acting on them.

2.4.1 ONE-MASS OR LUMPED MODEL

In the one-mass model, the drivetrain is assumed to be rigid, therefore both the rotor and generator rotate at the same speed (corrected with the gearbox ratio). The only degree of freedom present is chosen to be the rotation of the rotor, $\int_0^t \Omega_R(t) dt$, with $\Omega_R(t)$ being the rotational velocity of the rotor. The equation of motion of the drivetrain is given by Equation 2.5:

$$I_{DT} \dot{\Omega}_R(t) = T_{R;A;Y}(t) - N_{GB} T_G. \quad (2.5)$$

Where I_{DT} is the rotational inertia of the drivetrain (Table 2.1), $T_{R;A;Y}(t)$ the aerodynamic torque around the Y-axis acting on the rotor (Equation 3.2) and $N_{GB} T_G$ the rated electromagnetic generator torque converted to its low speed shaft equivalent (Table 2.2), note that the equivalent electromagnetic rotor torque is kept constant in the above rated regime. The rotational acceleration of the rotor is represented by $\dot{\Omega}_R(t)$. The rotational inertia of the total drivetrain is determined by Equation 2.6, in which I_R and I_G represent the rotational inertia of the rotor and generator, respectively, while N_{GB} represents the gearbox ratio (Table 2.1). The inertia of the generator is converted into its low speed shaft equivalent:

$$I_{DT} = I_R + N_{GB}^2 I_G. \quad (2.6)$$

An illustration of the model is presented in Figure 2.3, where the aerodynamic torque is defined as a positive

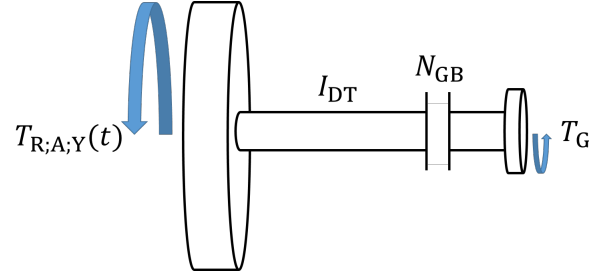


Figure 2.3: One-mass drivetrain model.

moment around the Y-axis coinciding with the drivetrain, while the generator torque is positively defined in the opposite direction. Note that the aerodynamic torque is dependent on both $\Delta\Omega_R(t)$ and $\int_0^t \Delta\Omega_R(t)dt$ directly and via the pitch controller and thus adds damping and stiffness to the system.

2.4.2 TWO-MASS MODEL

The two-mass model includes the stiffness and damping of the drivetrain, represented by K_{DT} and C_{DT} , which are evaluated for the low speed shaft. The rotor and generator both have their own degree of freedom since they are not rigidly connected. The rotational degree of freedom of the rotor is represented by $\int_0^t \Omega_R(t)dt$, while the degree of freedom of the high speed generator shaft is denoted by $\int_0^t \Omega_G(t)dt$. This results in the system of equation of motions presented in Equation 2.7:

$$\begin{bmatrix} I_R & 0 \\ 0 & I_G \end{bmatrix} \begin{bmatrix} \dot{\Omega}_R(t) \\ \dot{\Omega}_G(t) \end{bmatrix} + C_{DT} \begin{bmatrix} 1 & \frac{-1}{N_{GB}} \\ \frac{-1}{N_{GB}} & \frac{1}{N_{GB}^2} \end{bmatrix} \begin{bmatrix} \Omega_R(t) \\ \Omega_G(t) \end{bmatrix} + K_{DT} \begin{bmatrix} 1 & \frac{-1}{N_{GB}} \\ \frac{-1}{N_{GB}} & \frac{1}{N_{GB}^2} \end{bmatrix} \begin{bmatrix} \int_0^t \Omega_R(t)dt \\ \int_0^t \Omega_G(t)dt \end{bmatrix} = \begin{bmatrix} T_{R;A;Y}(t) \\ -T_G \end{bmatrix}. \quad (2.7)$$

The model is visualized in Figure 2.4, where the aerodynamic torque acting on the rotor is defined positive around the Y-axis, the generator torque is defined as positive in the opposing direction, and the gearbox is indicated by N_{GB} . The gearbox has an even number of stages, which means that the rotor and generator rotate

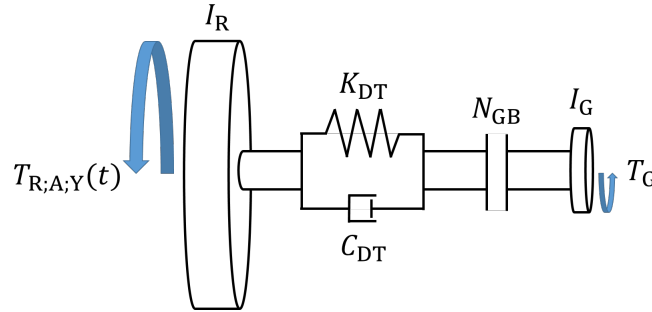


Figure 2.4: Two-mass drivetrain model.

in the same direction. It is assumed that there are no friction losses present in the drivetrain due to the bearing and gearbox.

2.5 INDUCTION FACTOR

The wind approaching a wind turbine is slowed down by its presence in the wind field. This means the wind velocity experienced by the rotor is lower than the upstream wind velocity. This effect is accounted for by the axial induction factor $a(r, t)$, as presented in Equation 2.8:

$$W_Y(r, t) = W_Y^\infty(t) \cdot \left(1 - a(r, t)\right), \quad (2.8)$$

where $W_Y(r, t)$ is the induced wind velocity at the rotor and $W_Y^\infty(t)$ is the upstream wind velocity. Since the wind field is assumed to be uniform, the upstream wind velocity is not space dependent. Besides this the wind field is assumed to only have a component in the Y-direction, thus only this component of the wind is considered. The axial induction factor varies over the length of the blades and with the wind velocity, hence it being dependent on time. Since the wind field is assumed to be uniform, the induction factor is identical for each blade. Three of the models that can be used to calculate the induction factor are the frozen, equilibrium and dynamic wake models [2] [1], which are presented below. The air passing through a rotor gains angular momentum due to the reaction torque applied on the air by the rotor, as a consequence the air particles in the wake will have a tangential velocity component which causes the wake to rotate in the direction opposite to that of the rotor. This effect can be taken into account via the tangential induction factor, however, this thesis neglects the wake rotation since it is assumed to have a small effect on the rotor behavior [2].

2.5.1 FROZEN WAKE MODEL

In the frozen wake model the axial induction factor is calculated for the average wind velocity (indicated by the bar) of the wind speed, \bar{W}_Y^∞ , corresponding mean pitch angle of the blades, β , and the rated rotational velocity of the rotor, $\bar{\Omega}_R$. Since the model is restricted to the above rated regime, the rotor velocity in equilibrium state is always equal to the rated rotor velocity. The axial induction factor is determined by equating the aerodynamic thrust acting on an annulus δr of the rotor swept area based on blade element theory and momentum theory. The definition of an annulus is visually presented in Figure 2.5. The aerodynamic thrust acting on an annulus

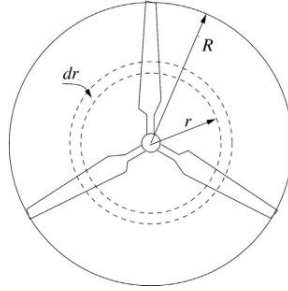


Figure 2.5: Annulus of the rotor swept area.

based on blade element theory is:

$$\delta F_Y = \frac{3}{2} \rho c(r) |\bar{\mathbf{W}}(r)|^2 \left(\left(C_L^c(r) + C_L^\alpha(r) \sin(\alpha(r)) \right) \cos(\phi(r)) + C_D(r) \sin(\phi(r)) \right) \delta r, \quad (2.9)$$

while momentum theory results in:

$$\delta F_Y = 4\pi\rho\{\bar{W}_Y^\infty\}^2 a(r) \left(1 - a(r)\right) r \delta r, \quad (2.10)$$

with

$$\alpha(r) = \arctan \left(\frac{\bar{W}_Y(r)}{\bar{\Omega}_R r} \right) - \beta_0(r) - \bar{\beta}, \quad (2.11)$$

and

$$\cos(\phi(r)) = \frac{\bar{\Omega}_R r}{|\bar{\mathbf{W}}(r)|}, \quad (2.12)$$

and

$$\sin(\phi(r)) = \frac{\bar{W}(r)}{|\bar{\mathbf{W}}(r)|}. \quad (2.13)$$

where $\alpha(r)$ is the angle of attack, and the inflow angle is represented by $\phi(r)$, which are defined according to Figure 2.6. The density of the air is denoted by ρ , the chord length of the airfoil by $c(r)$ and $\beta_0(r)$ describes the structural twist of the blades. $\bar{\mathbf{W}}(r)$ represents the relative velocity (not including structural motion) experienced by the airfoils, which depends on the wind speeds and rotational velocity and thus varies over the radius:

$$|\bar{\mathbf{W}}(r)| = \sqrt{\bar{\Omega}_R^2 r^2 + \bar{W}_Y(r)^2}. \quad (2.14)$$

The blades of the turbine are divided in different airfoil sections, as illustrated in Figure 2.7, the induction factor

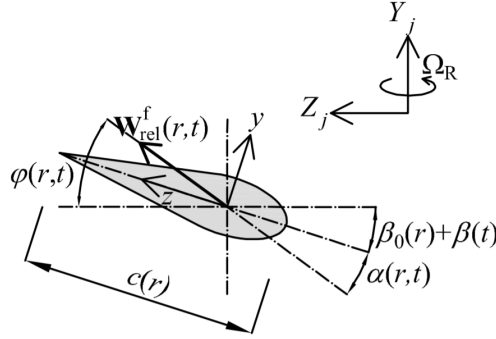


Figure 2.6: Definition of the inflow angle and angle of attack [10].

for each blade section, $a(r, t)$, is found by equating both the thrust force equations for the annulus that describes the particular blade section with the equation based on momentum theory. Since the frozen wake model is based on the mean operational parameters it is constant and can be determined at the start of the calculation of the model. This method is the least computationally expensive of the three presented and is obviously not an accurate description of the actual time dependent induction factor since the larger the deviation of the current wind velocity from the mean value, the larger the error of the induction factor becomes.

2.5.2 EQUILIBRIUM WAKE MODEL

The equilibrium wake model is based on the same equations as the frozen wake model but is not based on the mean 'frozen' operational parameters, instead the actual time dependent wind speed, rotational velocity and pitch angle are used. This results in the induction factor being evaluated at each time step and it thus becoming time dependent. This model assumes instant equilibrium after every change in wind velocity at every point in time. It is therefore suited for a wind signal step input in which the operational state to which the solution

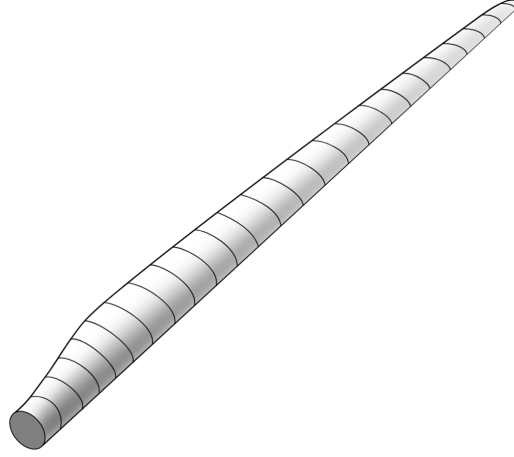


Figure 2.7: The different sections of the blade.

converges is important and the time it takes to converge less so, with exception of the study of the pitch control system.

2.5.3 DYNAMIC WAKE MODEL

The dynamic wake model introduces a time derivative of the axial induction factor, $\dot{a}(r, t)$ in the thrust equation based on momentum theory:

$$\delta F_Y(t) = 4\pi\rho\{W_Y^\infty(t)\}^2 a(r, t) \left(1 - a(r, t)\right) r \delta r + \frac{8}{3}\rho R^3 W_Y^\infty(t) \dot{a}(r, t). \quad (2.15)$$

The coefficient of $8/3$ of the added mass term is generally accepted [2]. Combined with the blade element theory thrust equation, the rate of change of the induction factor can be evaluated at each time step.

$$\dot{a}(r, t) = \left(\frac{3}{2}\rho c(r) |\mathbf{W}(t, r)|^2 \left((C_L^c(r) + C_L^\alpha(r) \sin(\alpha(t))) \cos(\phi(t)) + C_D(r) \sin(\phi(t)) \right) \delta r - 4\pi\rho\{W_Y^\infty(t)\}^2 a(r, t) (1 - a(r, t)) r \delta r \right) / \left(\frac{8}{3}\rho R^3 W_Y^\infty(t) \right) \quad (2.16)$$

This model takes into account the change in blade loading and the time it takes to change the induced flow field and is therefore best suited when realistic turbulent wind signals are used, however, adds to the computational expense of a model since this equation needs to be solved by time integration for each section, at each time step.

2.6 REFERENCE WIND TURBINE AND SUPPORT STRUCTURE

The wind turbine of which the specifications are used as input to generate results is the NREL 5-MW Reference Wind Turbine used for offshore system development from the National Renewable Energy Laboratory of the

United States Department of Energy [7]. This wind turbine is a conventional three-bladed upwind variable-speed variable blade-pitch-to-feather-controlled turbine, and is used as a reference by research teams worldwide. Several important specifications and operational parameters are presented in Table 2.1 and 2.2. More detailed specifications and parameters related to the blade sections can be found in Appendix A.

Description	Symbol	Value
Inertia hub	I_H	115,926 kgm ²
Inertia blade	I_B	12,857,000 kgm ²
Inertia rotor	I_R	38,686,000 kgm ²
Inertia generator	I_G	534.12 kgm ²
Inertia drivetrain	I_{DT}	43,712,000 kgm ²
Gearbox ratio	N_{GB}	97
Equivalent shaft torsional spring constant	K_{DT}	867,637,000 Nm/rad
Equivalent shaft torsional damping constant	C_{DT}	6,215,000 Nm/(rad/s)

Table 2.1: General specifications of the rotor and drivetrain [7].

Parameter	Symbol	Value
Above rated wind velocity regime	W	11.4 - 25.0 m/s
Rated rotational velocity rotor	$\bar{\Omega}_R$	1.267 rad/s
Rated rotational velocity generator	$\bar{\Omega}_G$	122.910 rad/s
Electromagnetic generator torque	T_G	43,093 Nm
Proportional gain	K_P	0.008449
Integral gain	K_I	0.004457

Table 2.2: The operational parameters in the above rated regime [7].

The offshore monopile support structure is modeled as a discretized cantilever beam based on the reference monopile structure defined in [3]. The support structure is designed for a North Sea site with a water depth of approximately 25 meters. The outer diameter varies from 5.6 m at the bottom to 4 m at the top, while the wall thickness varies from 32 mm at the tower base to 20 mm at the top.

2.7 WIND SIGNALS

In this thesis, a step input wind signal and turbulent wind signal are considered. These signals are input for the numerical models to generate results. The step signal is used to check the convergence of the parameters to a new equilibrium state, while the turbulent signal represents a more realistic input signal. The wind signals are single point history signals, evaluated at hub height, this means they are uniform over the rotor. It is assumed that the wind velocity field only has a component perpendicular to the XZ-plane (see Figure 2.1). Since all results are generated for a 15 m/s mean wind velocity the step input runs from 13 to 17 m/s with increments of 1 m/s wind velocity. The duration of each step is chosen to be 25 seconds, since this is long enough for a new equilibrium to be established. The turbulent signal is generated by Bladed for a mean wind velocity of 15 m/s and using a Kaimal spectrum, which describes the turbulent behavior of wind. The turbulence is frozen, which means the entire wind field is generated beforehand, and does not change in time. Since the wind only has one directional component (in the direction of the Y-axis), it only has one length scale. The length scale describes the size of the large energy-containing eddies in a turbulent flow, and is chosen to be 340.2 m. The turbulence

intensity is defined as the standard deviation divided by the mean wind velocity, and for the particular turbulent signal used, equal to 15.7267%, which is considered a high-turbulence signal. Both signals used are presented in Figure 2.8

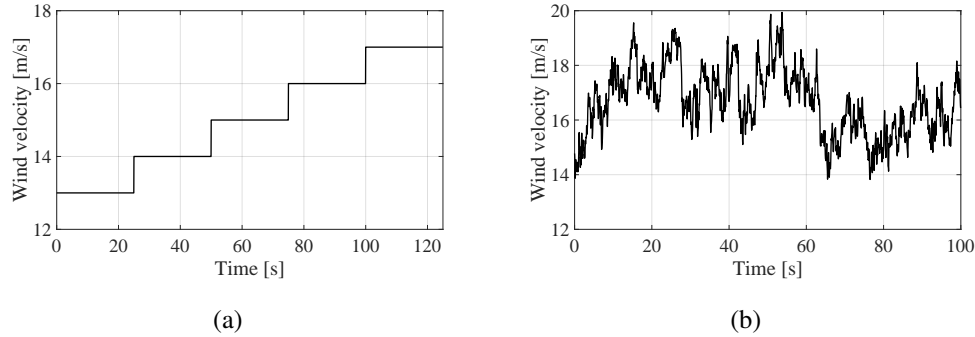


Figure 2.8: The step (a) and turbulent (b) wind signals used to generate results.

2.8 ASSUMPTIONS AND LIMITATIONS

The models that are presented in subsequent chapters are simplified by making several assumptions, the first of which is the wind only having an axial component in the Y direction and being uniform. The second assumption is the flow being attached to the surface of the blades, so no flow separation will occur, this is a valid assumption for low angles of attack. The wake is assumed to be non rotating, and thus the tangential induction factor is not included in the model, which is a reasonable assumption without a significant effect on the behavior of the model based on [2]. The dynamics of the pitch control system is not included in the models, the gains used are taken from Bladed. The drivetrain is assumed to have no friction losses, and the blades of the rotor are assumed to be rigid and identical. The results are generated in the above rated operation regime of the wind turbine in which only the blade pitch controller is active, therefore, there is no generator torque controller included in the model (which is active for below rated wind speeds). Besides this, the model does not include any hydrodynamic loading.

3 | RIGID DRIVETRAIN MODEL WITH NONLINEAR AERODYNAMIC TORQUE

In this chapter the rotor and drivetrain model is presented. Matlab results are generated for both a step wind input and a turbulent wind input and the model is validated by comparing these results to Bladed results generated with the same input. Some simplifications of the model are investigated and commented upon.

3.1 MODEL DESCRIPTION

Based on the assumptions that the tower top is fixed and has no motions and the drivetrain shaft is rigid, the only degree of freedom present is the rotation of the drivetrain, $\int \Omega(t)_R dt$, with $\Omega_R(t)$ being the rotational velocity of the rotor. The equation of motion of the drivetrain is as follows, based on the one-mass model as described in Section 2.4.1:

$$I_{DT}\dot{\Omega}_R(t) = T_{R;A;Y}(t) - N_{GB}T_G. \quad (3.1)$$

The electromagnetic generator torque is constant in the above rated regime.

3.1.1 AERODYNAMIC TORQUE AND THRUST FORCE

The aerodynamic torque, $T_{R;A;Y}(t)$, and thrust force, $F_{R;A;Y}(t)$, acting on a rotor with three identical blades are defined in [10]. The thrust force is not included in this model, since the only degree of freedom present is the rotation of the drivetrain, however, it is presented here since the thrust force is used for validation purposes. Both the thrust force and aerodynamic torque acting are divided in an angle of attack dependent lift contribution, a lift component related to the cambered shape of the airfoils, and a drag contribution:

$$T_{R;A;Y}(t) = T_{R;L;Y}^\alpha(t) + T_{R;L;Y}^c(t) + T_{R;D;Y}(t) \quad (3.2)$$

and

$$F_{R;A;Y}(t) = F_{R;L;Y}^\alpha(t) + F_{R;L;Y}^c(t) + F_{R;D;Y}(t), \quad (3.3)$$

where the components corresponding to the angle of attack are:

$$\begin{aligned} T_{R;L;Y}^\alpha(t) = & 3/2 \int_{r_0}^R \rho c(r) C_L^\alpha(r, t) \cos(\beta_0(r) + \beta(t)) r \{W_Y(r, t)\}^2 dr \\ & - 3/2 \int_{r_0}^R \rho c(r) C_L^\alpha(r, t) \sin(\beta_0(r) + \beta(t)) \Omega_R(t) r^2 W_Y(r, t) dr \end{aligned} \quad (3.4)$$

and

$$F_{R;L;Y}^\alpha(t) = 3/2 \int_{r_0}^R \rho c(r) C_L^\alpha(r, t) \cos(\beta_0(r) + \beta(t)) \Omega_R(t) r W_Y(r, t) dr - 3/2 \int_{r_0}^R \rho c(r) C_L^\alpha(r, t) \sin(\beta_0(r) + \beta(t)) \Omega_R(t)^2 r^2 dr. \quad (3.5)$$

The excitation component related to the camber of the airfoils are defined as:

$$T_{R;L;Y}^c(t) = 3/2 \int_{r_0}^R \rho c(r) C_L^c(r) |\mathbf{W}(r, t)| r W_Y(r, t) dr \quad (3.6)$$

and

$$F_{R;L;Y}^c(t) = 3/2 \int_{r_0}^R \rho c(r) C_L^c(r) |\mathbf{W}(r, t)| \Omega_R(t) r dr. \quad (3.7)$$

And the parts corresponding to the drag force generated by the rotor are described as:

$$T_{R;D;Y}(t) = -3/2 \int_{r_0}^R \rho c(r) C_D(r, t) |\mathbf{W}(r, t)| \Omega_R(t) r^2 dr \quad (3.8)$$

and

$$F_{R;D;Y}(t) = 3/2 \int_{r_0}^R \rho c(r) C_D(r, t) |\mathbf{W}(r, t)| W_Y(r, t) dr, \quad (3.9)$$

where ρ is the air density, $c(r)$ and $\beta_0(r)$ are the chord length and structural twist of the blades, respectively (Table A.1), and r represents the distance to the center of the hub along the blade. The lift and drag coefficients are represented by $C_L^c(r)$, $C_L^\alpha(r, t)$, and $C_D(r, t)$ (Table A.2, A.3 and A.4). The pitch angle is defined as $\beta(t)$ and the rotational velocity is represented by $\Omega_R(t)$. The induced wind velocity is denoted by $W_Y(r, t)$ while the relative velocity $|\mathbf{W}(r, t)|$ is defined as follows:

$$|\mathbf{W}(r, t)| = \sqrt{\Omega_R(t)^2 r^2 + W_Y(r, t)^2} \quad (3.10)$$

The forces and moments are integrated over the length of the blades from r_0 to R , which are the distances from the root and tip of the blade to the center of the hub. The wind velocity as presented in Equation 3.3 to 3.8 contains the multiplication with the induction factor a :

$$W_Y(r, t) = W_Y^\infty(t) (1 - a(r, t)), \quad (3.11)$$

where $W_Y^\infty(t)$ is the wind velocity far from the wind turbine.

3.1.2 LIFT AND DRAG COEFFICIENTS

Since the wind velocity is time dependent, the parameters that are wind velocity dependent will also be time dependent. As a result, the angle of attack dependent lift coefficient $C_L^\alpha(r, t)$ and the drag coefficient $C_D(r, t)$ should be updated every time step with varying wind velocity. The lift and drag coefficients are updated by interpolating the values of Table A.3 and A.4 to the current wind velocity.

3.2 VALIDATION

The model is implemented in Matlab and validated by comparing its results to results generated with DNV GL's commercial wind turbine simulation tool Bladed. All the input parameters of the model both used in Matlab and Bladed can be found in Chapter 2 and Appendix A. First, the different components of the aerodynamic torque and their sum is calculated for each operational state in the above rated regime. Afterwards, two wind input signals are considered; a step input and a turbulent input. By using a step input signal it can be easily observed whether the solution converges to the right equilibrium states or not, while the turbulent input represents a more realistic wind signal. Finally, the validity of the small angle of attack assumption, mentioned in the previous chapter, is checked.

3.2.1 NUMERICAL MODEL

The equations and specifications previously given are used to create a Matlab model in which the following set of differential equations are solved using the ODE45 function based on the Runge-Kutta method.

$$\left\{ \begin{array}{l} \Delta \dot{\Omega}_R(t) = (T_{R:A;Y}(\Delta \Omega_R(t), \Delta \beta(t), t) - N_{GB}T_G)/I_{DT} \\ \Delta \dot{\beta}(t) = K_P N_{GB}(T_{R:A;Y}(\Delta \Omega_R(t), \Delta \beta(t), t) - N_{GB}T_G)/I_{DT} + K_I N_{GB} \Delta \Omega_R(t) \\ \dot{\mathbf{a}}(t) = \text{Equation 2.16} \end{array} \right\}$$

The induction is solved for each blade section by using Equation 2.16 and thus it has the same length as the number of blade sections used in the model. Note that the time derivative of the induction factor is only necessary to be included in this system of equations when the dynamic wake model is used.

3.2.2 AERODYNAMIC TORQUE COMPONENTS FOR DIFFERENT OPERATIONAL STATES

The aerodynamic torque components presented in Equation 3.2 to 3.8 are evaluated at different operational states in the above rated regime. An operational state is defined as an equilibrium state where the rotor rotates at the rated rotational velocity and the aerodynamic torque acting on the rotor is equal and opposite to the equivalent electromagnetic generator torque. This equilibrium for a certain wind velocity, thus contains a corresponding aerodynamic torque, rotational velocity, lift and drag coefficients, pitch angle and induction factor. For wind speeds varying from 12 m/s to 25 m/s (the above rated regime), the corresponding equilibrium pitch angle (Table A.5), the rated rotational velocity and the corresponding induction based on the equilibrium wake model (Section 2.5.2) are used. At any operational state, the sum of the three components of the aerodynamic torque should be constant and equal to the equivalent rated generator torque (including the gearbox ratio) of 4.18 MNm, which can be concluded from Figure 3.1. The drag component of the torque is negative and relatively small. The lift component that is dependent on the angle of attack is positive for lower winds speeds, but decreases with increasing wind speed and ultimately becomes negative. The lift component related to the camber of the airfoils is positive and increases with increasing wind velocity. It can be seen that the increase of the pitch angle for higher wind velocities, and thus the increase in size of the angle of attack related torque component, compensates for the increase in lift due to the cambered shape of the airfoil for increasing wind speed, and thus keeping the wind turbine operational for increasing wind velocity. Since the sum of the three components is equal to the equivalent generator torque for each operational state in the above rated wind regime, the model is in equilibrium at each state. To generate these results the equilibrium pitch angles provided by Bladed are used, to check whether the controller converges to these values a step wind input signal is used, of which the results are presented in the following section.

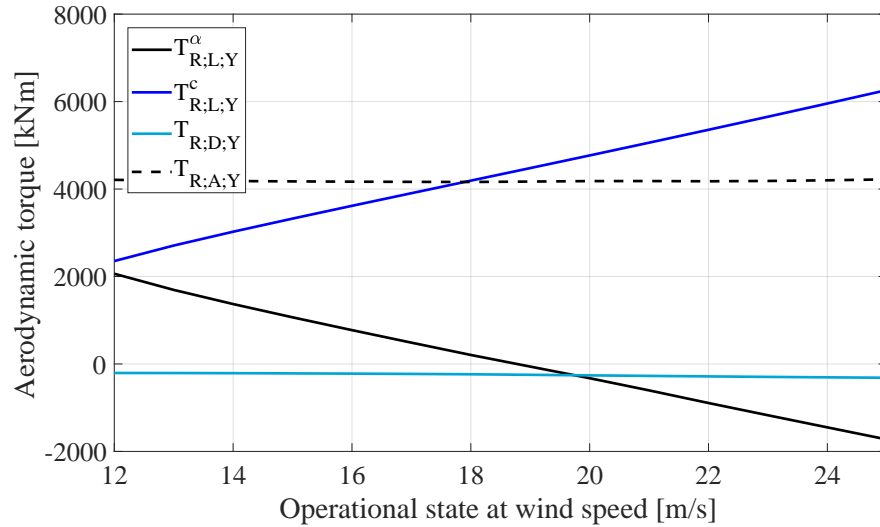


Figure 3.1: The different components of the aerodynamic torque for operational states throughout the above rated regime.

3.2.3 STEP WIND INPUT SIGNAL

For a wind step input (Figure 3.4.a) it can be observed that with each increasing step in wind velocity the rotational velocity increases (Figure 3.4.b), which triggers the pitch controller to increase the pitch angle and bring the rotational velocity back to its rated rotational speed. From Figure 3.4.c it can be concluded that the Matlab model converges to the same pitch angles in equilibrium positions (represented by the black lines marked with its corresponding wind velocity) as the values provided by Bladed (Table A.5). For these pitch angles at the corresponding wind velocities and rated rotational velocity the aerodynamic torque acting on the rotor is equal to the equivalent electromagnetic torque of the generator, acting in the opposite direction. As a result, the net torque acting on the drivetrain is zero and thus the rotational velocity is constant: the rated rotational velocity. The increase in equilibrium pitch angle for 1 m/s increase in wind speed decreases, because the sensitivity of the aerodynamic torque to the pitch angle increases for higher pitch angles, this explains the behavior observed in Figure 3.4.b. The torque acting on the rotor can be observed to converge back to the value of the equivalent electromagnetic generator torque after each step in wind speed. The increasing height of the torque spike caused by each step increase in wind speed (Figure 3.4.d) is a result of the non-linear dependency of the torque on the wind velocity, as presented in Equation 3.2 to 3.8. The thrust force, on the other hand, decreases with increasing wind speeds since the pitch angle becomes larger which decreases the area exposed to the wind in fore-aft direction, as can be seen in Figure 3.4.e. To obtain the results for a step input wind signal the equilibrium wake model is used (Section 2.5.2), the initial values of the rotational velocity of the rotor is the rated velocity, while the initial pitch angle is equal to the pitch angle corresponding to an equilibrium state at a wind velocity of 13 m/s.

3.2.4 TURBULENT WIND INPUT SIGNAL

For the turbulent wind input (Figure 3.5.a) the rotational velocity and pitch angle show very similar behavior in Figure 3.5.b and 3.5.c, respectively. The aerodynamic torque (Figure 3.5.d) can be seen to move around the equivalent electromagnetic generator torque, which is the aerodynamic torque that is controlled for. The thrust force found with the Matlab model and Bladed are in good correspondence, see Figure 3.5.e. The results for a turbulent wind input signal are obtained by using the dynamic wake model (Section 2.5.3). Since the turbulent wind input signal was generated for a mean wind speed of 15 m/s, the initial values of all time dependent parameters are those corresponding to the operational state at a wind velocity of 15 m/s.

3.2.5 LOW ANGLE OF ATTACK ASSUMPTION

As mentioned in Chapter 2, the lift coefficient is split up in a part dependent on the cambered shape of the airfoil, and a part dependent on the angle of attack. The relation as presented is only valid for low angles of attack. For the turbulent wind signal input, the highest occurring angle of attack at the center of each blade section is determined, and presented in Figure 3.2. As can be seen in Figure 3.3, the linear relation between the

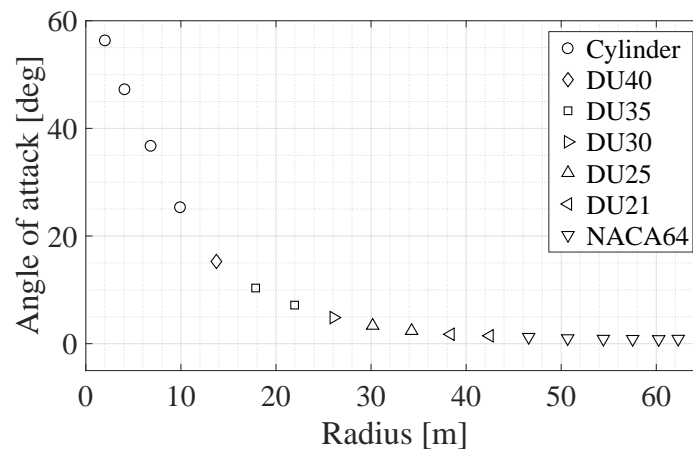


Figure 3.2: The highest occurring angle of attack during the turbulent wind signal at the center of each blade section, with the corresponding airfoils.

lift coefficient and the angle of attack is valid for an angle of attack of approximately -5 to 10 degrees. Only the five blade sections closest to the hub of the rotor experience angles of attack larger than 10 degrees (see Figure 3.2). Four of these sections have a cylindrical shape, and thus produce no lift. The fifth section from the hub experiences an angle of attack of 15 degrees, which lies outside the linear region, however the linear relation is used, which is a cause for differences found between Bladed and the model.

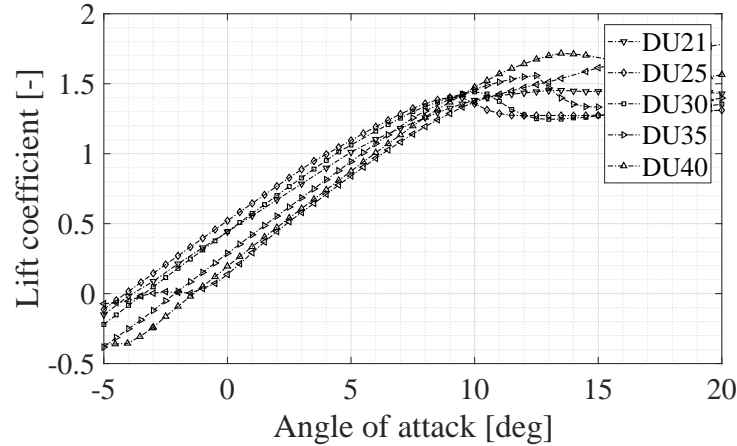


Figure 3.3: The lift coefficient for varying angle of attack of the different airfoils.

3.3 MODEL SIMPLIFICATION

This section investigates possible simplifications of the model. The time dependent parameters of the model are the wind velocity, rotational velocity, pitch angle, induction factor and lift and drag coefficients. Obviously, the wind velocity and rotational velocity must be time dependent to obtain any non trivial results. Besides this, the pitch angle has to be time dependent for the pitch controller to be able to operate. The necessity of the time dependency of the induction factor and lift and drag coefficients are investigated in this section.

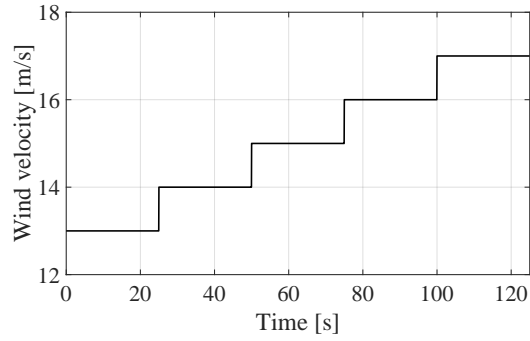
3.3.1 CONSTANT LIFT AND DRAG COEFFICIENTS

In the previously presented results (Figure 3.4 and 3.5), the lift and drag coefficients are drawn from a look-up table at each time step (Table A.3 and A.4). To eliminate the need for look-up tables and to reduce the computational time, constant coefficients are proposed. The coefficients are evaluated at the mean operational state and kept constant throughout the calculation, and results are generated for a step and turbulent wind input. For the step input (Figure 3.6.a) it can be seen that taking the lift and drag coefficients constant has no significant effect on the rotational velocity and pitch angle found, see Figure 3.6.b and 3.6.c. Based on this, it is expected that the same is observed for a turbulent wind signal (Figure 3.7.a). Indeed, the rotational velocity and pitch angle for the turbulent input signal show no significant deviation from the ones obtained by using time varying lift and drag coefficients. Based on these results it is concluded that the lift and drag coefficients can be evaluated for the mean wind velocity of the signal, and thus becoming time independent, without it having any significant effect on the solutions found.

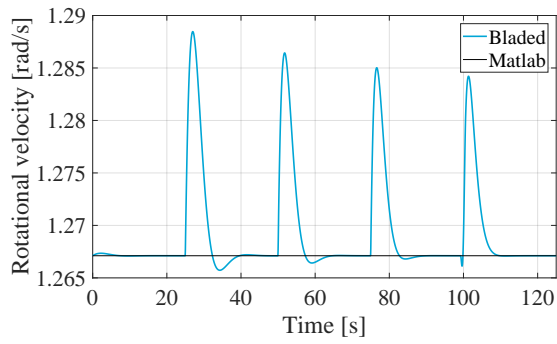
3.3.2 FROZEN WAKE MODEL

To eliminate the time dependency of the induction factor and reduce computational expense, the frozen wake model described in Section 2.5.1 can be used. In this case the induction factor is not calculated at each time step,

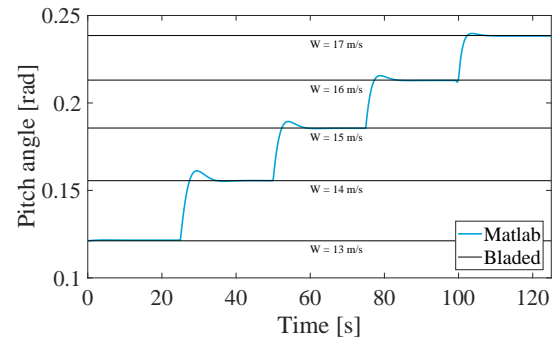
but beforehand for the operational state corresponding to the chosen mean value of the wind signal and kept constant throughout the calculation. First, a step wind input is considered (Figure 3.6.a), because the induction factor corresponding to a wind velocity of 15 m/s is used it takes time for a new equilibrium to establish itself. For wind speeds below 15 m/s the induction factor is underestimated, resulting in an overestimation of the actual wind velocity. This in turn results in the pitch angle being too high, this reasoning can be reversibly applied to the situation where the wind is higher than 15 m/s, as can be seen in Figure 3.6.e. Because the increment between the subsequent pitch angles for which equilibrium is found is smaller than is the case when the equilibrium wake model is used, the peaks in rotational velocity are smaller (Figure 3.6.c). For a turbulent wind input (Figure 3.7.a), the use of the frozen wake model does not significantly affect the result of the rotational velocity of the rotor, as can be seen in Figure 3.7.c. Figure 3.7.e shows that the pitch angle is underestimated when the frozen wake model is used because the wind velocity is mostly higher than the operational state at which the induction factor is evaluated, as is also seen in Figure 3.6.e. This results in overestimation of the thrust force. Since an accurate approximation of the thrust force is necessary when a support structure, and thus tower top motion, is included to predict said motion, it is concluded that the frozen wake model does not give desirable results and therefore, from now on, only the equilibrium and dynamic wake models are used.



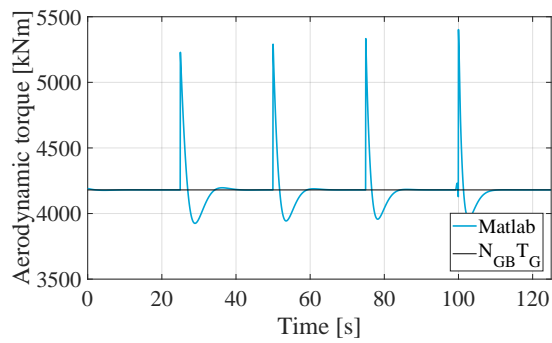
(a)



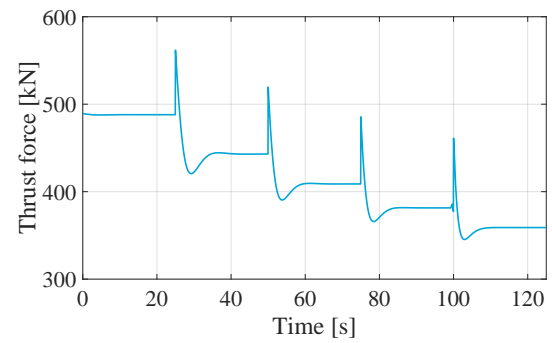
(b)



(c)



(d)



(e)

Figure 3.4: Results for step wind input with wind signal (a), rotational velocity (b), pitch angle (c), aerodynamic torque (d) and thrust force (e).

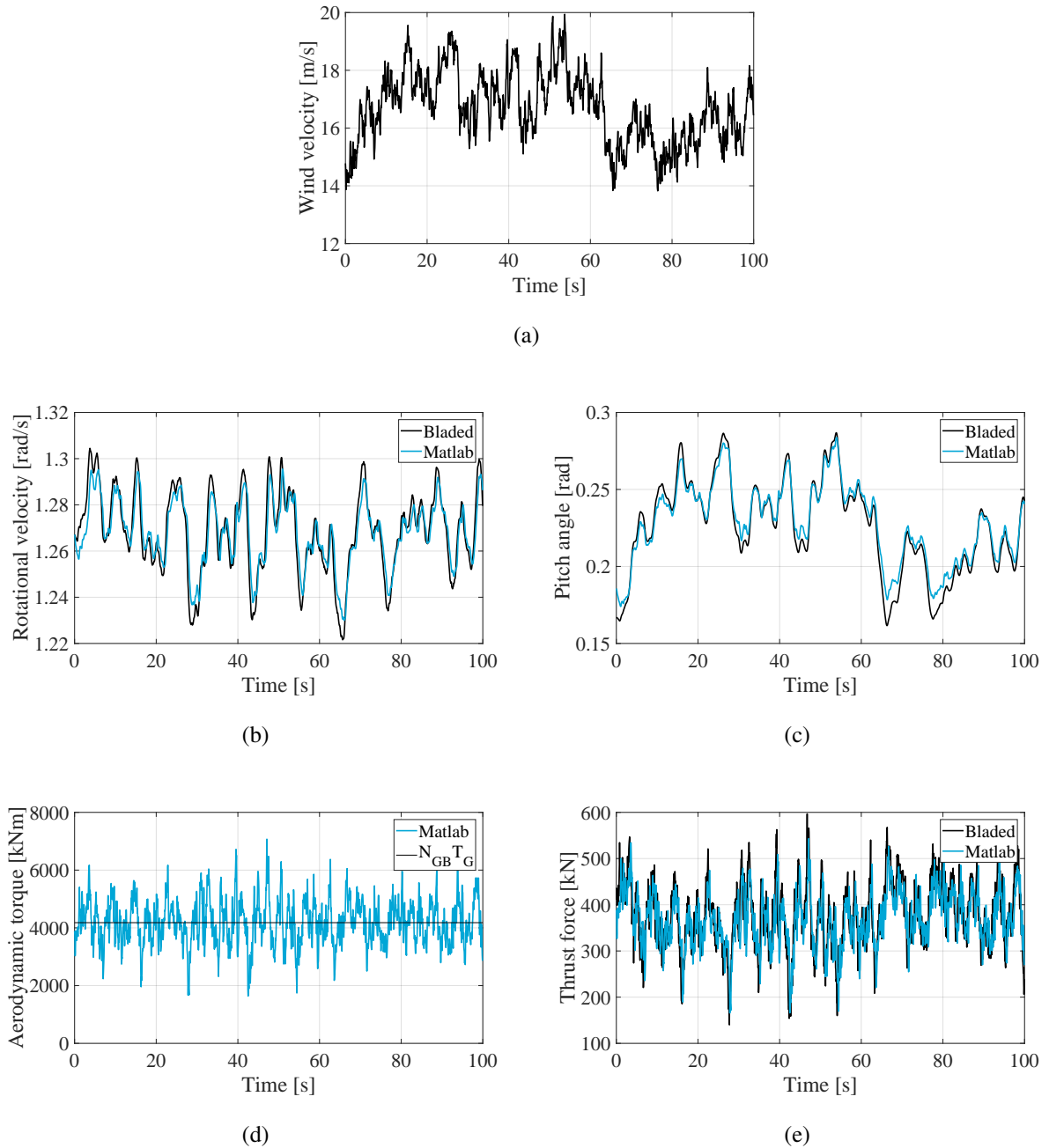


Figure 3.5: Results for turbulent wind input with wind signal (a), rotational velocity (b), pitch angle (c), aerodynamic torque (d) and thrust force (e).

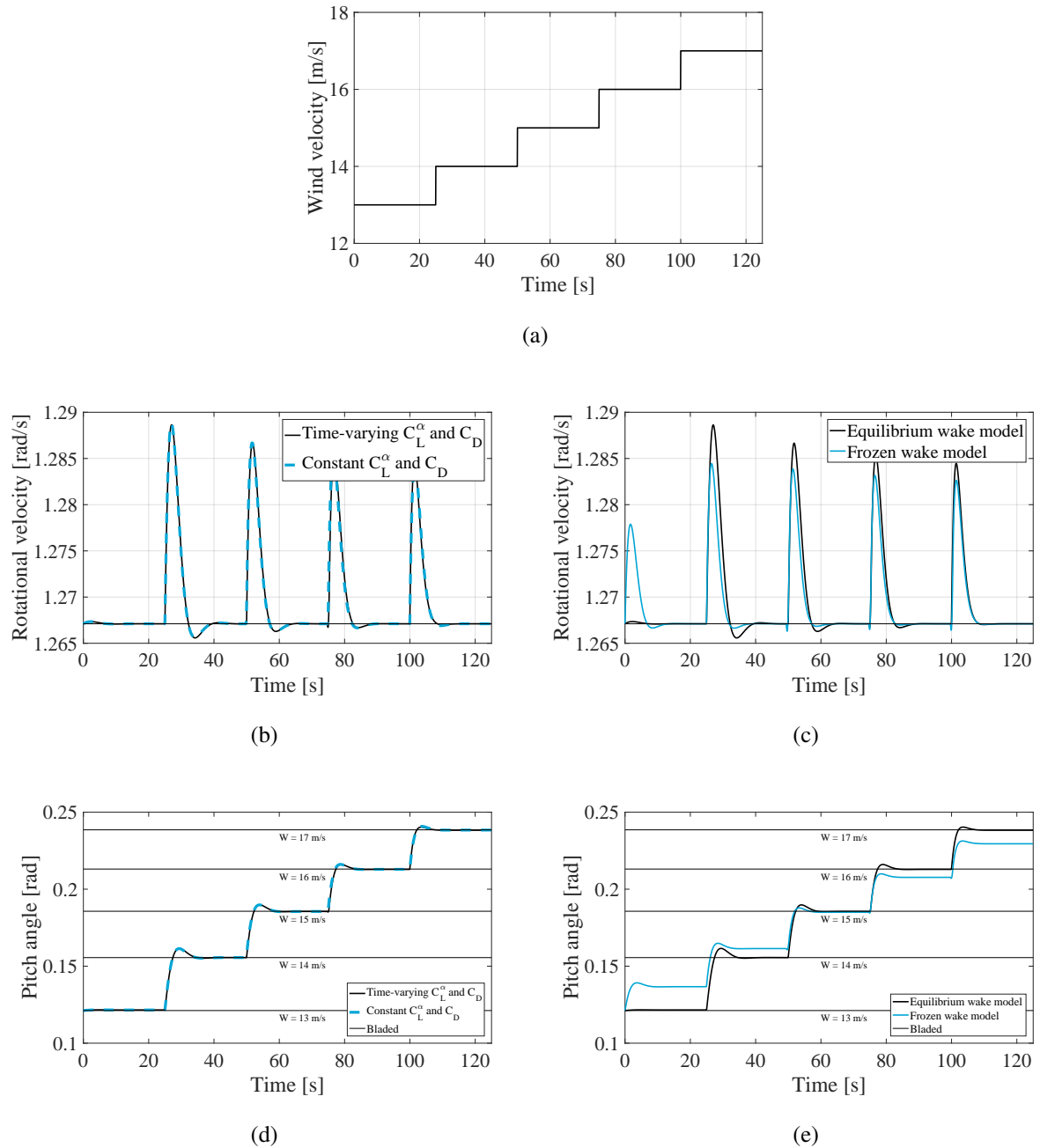


Figure 3.6: Results for step wind input with wind signal (a), rotational velocity (b), pitch angle (d) for time varying coefficients and constant coefficients and rotational velocity (c) and pitch angle (e) for the dynamic wake model and frozen wake model.

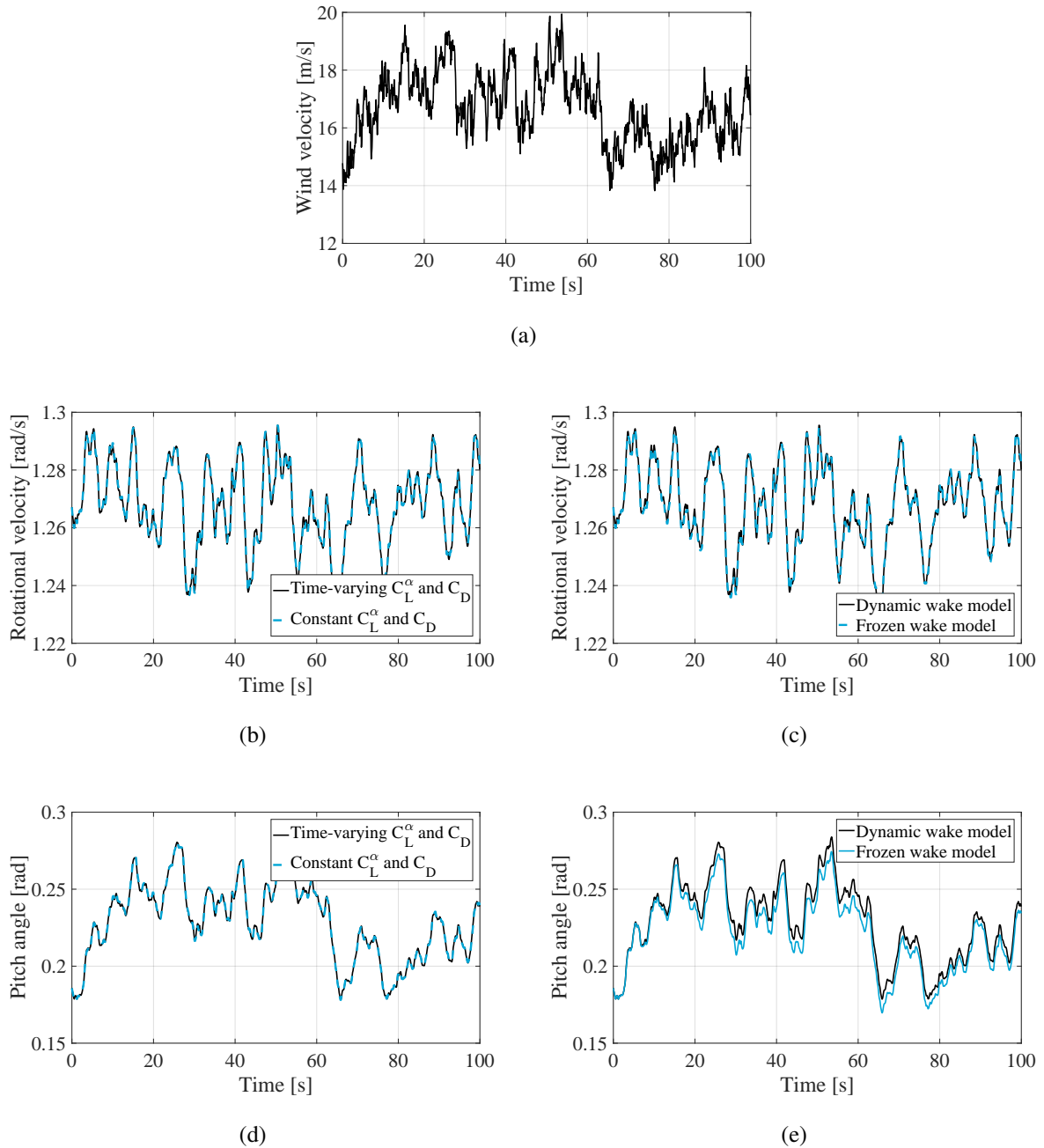


Figure 3.7: Results for turbulent wind input with wind signal (a), rotational velocity (b), pitch angle (d) for time varying coefficients and constant coefficients and rotational velocity (c) and pitch angle (e) for the dynamic wake model and frozen wake model.

4 | RIGID DRIVETRAIN MODEL WITH LINEARIZED AERODYNAMIC TORQUE

In this chapter a rotor and drivetrain model with linearized (with respect to wind speed, rotational velocity, pitch angle and axial inflow factor) aerodynamic excitation is presented. The aerodynamic torque acting on the drivetrain will be approximated by use of a first order Taylor series expansion around a certain operation point, and the results of the model are analyzed and compared to the nonlinear excitation model described in Chapter 3.

4.1 LINEARIZED APPROXIMATION OF THE AERODYNAMIC TORQUE

Recalling Equation 2.5, the equation of motion of the drivetrain, a linearized approximation of the aerodynamic torque is presented:

$$I_{DT}\dot{\Omega}_R(t) = T_{R;A;Y}(t) - N_{GB}T_G. \quad (4.1)$$

In this model, the wind speed, rotational velocity, pitch angle and axial induction factor are separated in a mean value (indicated by the bar) and a time-varying deviation from it. Based on the results found in Section 3.3.1 the angle of attack dependent lift coefficient $C_L^\alpha(r, t)$ and drag coefficient $C_D(r, t)$ are assumed to be time independent.

$$W_Y(r, t) = \bar{W}_Y(r) + \Delta W_Y(r, t) \quad (4.2)$$

$$\Omega_R(t) = \bar{\Omega}_R + \Delta\Omega_R(t) \quad (4.3)$$

$$\beta(t) = \bar{\beta} + \Delta\beta(t) \quad (4.4)$$

$$a(r, t) = \bar{a}(r) + \Delta a(r, t), \quad (4.5)$$

where $\bar{\Omega}_R$ is equal to the rated rotational velocity (since the model restricts itself to the above rated regime), $\bar{\beta}$ and $\bar{a}(r)$ are equal to the operational pitch angle (Table A.5) and axial induction factor corresponding to wind velocity $\bar{W}_Y(r)$, respectively. The mean velocity $\bar{W}_Y(r)$ does not necessarily have to be the actual mean value of the wind input signal, but it represents the mean wind velocity value for which the random turbulent signal is generated. Based on Equation 4.2 to 4.5 an operating point S is specified. This operational state S represents an equilibrium position corresponding to the wind velocity $\bar{W}_Y(r)$, where there is no resultant torque present and the drivetrain thus rotates at a constant speed (the rated velocity $\bar{\Omega}_R$):

$$S = \left\{ W_Y(t, r) = \bar{W}_Y(r), \Omega_R(t) = \bar{\Omega}_R, \beta(t) = \bar{\beta}, a(r, t) = \bar{a}(r) \right\}. \quad (4.6)$$

In a similar way as for the variables above, the aerodynamic torque is separated in a mean value evaluated at point S and a fluctuating component:

$$T_{R;A;Y}(t) = \bar{T}_{R;A;Y} + \Delta T_{R;A;Y}(t). \quad (4.7)$$

Based on the definition of point S and the operational equilibrium of the drivetrain, the value of the aerodynamic torque evaluated at point S is equal to the equivalent electromagnetic generator torque in the above rated wind regime, $N_{GB}T_G$:

$$\bar{T}_{R;A;Y} = T_{R;A;Y}(t) \Big|_S = N_{GB}T_G, \quad (4.8)$$

this results in a simplified equation of motion:

$$I_{DT}\dot{\Omega}_R(t) = \Delta T_{R;A;Y}(t). \quad (4.9)$$

The time-varying part of the aerodynamic torque is dependent on the wind speed, rotational velocity, pitch angle of the blades and the induction factor, and is thus approximated by the following first order Taylor series expansion:

$$\Delta T_{R;A;Y}(t) \approx \frac{\partial T_{R;A;Y}(t)}{\partial W_Y(r, t)} \Big|_S \Delta W_Y(r, t) + \frac{\partial T_{R;A;Y}(t)}{\partial \Omega(t)} \Big|_S \Delta \Omega(t) + \frac{\partial T_{R;A;Y}(t)}{\partial \beta(t)} \Big|_S \Delta \beta(t) + \frac{\partial T_{R;A;Y}(t)}{\partial a(r, t)} \Big|_S \Delta a(r, t). \quad (4.10)$$

In the following subsections each partial derivative is presented and evaluated over a range of states in the above rated regime. The value and slope of partial derivative are commented upon.

4.1.1 AERODYNAMIC TORQUE SENSITIVITY TO WIND SPEED VARIATIONS

As is done in Section 3.1.1, the torque is split up in three parts, where the partial derivative of the torque with respect to the wind velocity is equal to the sum of the partial derivatives of the components:

$$\frac{\partial T_{R;A;Y}(t)}{\partial W_Y(r, t)} \Big|_S = \frac{\partial T_{R;L;Y}^\alpha(t)}{\partial W_Y(r, t)} \Big|_S + \frac{\partial T_{R;L;Y}^c(r, t)}{\partial W_Y(r, t)} \Big|_S + \frac{\partial T_{R;D;Y}(t)}{\partial W_Y(r, t)} \Big|_S, \quad (4.11)$$

where the partial derivative of the angle of attack dependent part of the aerodynamic torque to the wind velocity is:

$$\begin{aligned} \frac{\partial T_{R;L;Y}^\alpha(t)}{\partial W_Y(r, t)} \Big|_S &= -\frac{3}{2} \int_{r_0}^R \rho c(r) C_L^\alpha(r) \sin(\beta_0(r) + \bar{\beta}) \bar{\Omega}_R r^2 dr \\ &+ 3 \int_{r_0}^R \rho c(r) C_L^\alpha(r) \cos(\beta_0(r) + \bar{\beta}) \bar{W}_Y(r) r dr, \end{aligned} \quad (4.12)$$

and the partial derivative related to the cambered shape of the airfoils is:

$$\begin{aligned} \frac{\partial T_{R;L;Y}^c(t)}{\partial W_Y(r, t)} \Big|_S &= \frac{3}{2} \int_{r_0}^R \rho c(r) C_L^c(r) |\bar{\mathbf{W}}(r)| r dr \\ &+ \frac{3}{2} \int_{r_0}^R \frac{\rho c(r) C_L^c(r)}{|\bar{\mathbf{W}}(r)|} \{\bar{W}_Y(r)\}^2 r dr, \end{aligned} \quad (4.13)$$

and finally, the sensitivity of the drag related torque to the wind speed is described as:

$$\frac{\partial T_{R;D;Y}(t)}{\partial W_Y(r, t)} \Big|_S = -\frac{3}{2} \int_{r_0}^R \frac{\rho c(r) C_D(r)}{|\bar{\mathbf{W}}(r)|} \bar{\Omega}_R r^2 \bar{W}_Y(t) dr. \quad (4.14)$$

The sensitivity of the aerodynamic torque to changes in the wind speed is plotted for different operational states in the above rated regime in Figure 4.1.a. It can be observed that it is positive, as expected, and increases with increasing wind speed. Its linear nature results from a second order dependency of the torque to the wind velocity.

4.1.2 AERODYNAMIC TORQUE SENSITIVITY TO ROTATIONAL VELOCITY VARIATIONS

The sensitivity of the aerodynamic torque to the rotational velocity of the rotor is split up into three components:

$$\left. \frac{\partial T_{R:A;Y}(t)}{\partial \Omega_R(t)} \right|_S = \left. \frac{\partial T_{R:L;Y}^\alpha(t)}{\partial \Omega_R(t)} \right|_S + \left. \frac{\partial T_{R:L;Y}^c(t)}{\partial \Omega_R(t)} \right|_S + \left. \frac{\partial T_{R:D;Y}(t)}{\partial \Omega_R(t)} \right|_S, \quad (4.15)$$

where the first lift component, depending on the angle of attack, is described by Equation 4.16:

$$\left. \frac{\partial T_{R:L;Y}^\alpha(t)}{\partial \Omega_R(t)} \right|_S = -\frac{3}{2} \int_{r_0}^R \rho c(r) C_L^\alpha(r) \sin(\beta_0(r) + \bar{\beta}) \bar{W}_Y(r) r^2 dr. \quad (4.16)$$

The sensitivity related to the camber of the airfoils is defined as:

$$\left. \frac{\partial T_{R:L;Y}^c(t)}{\partial \Omega_R(t)} \right|_S = \frac{3}{2} \int_{r_0}^R \frac{\rho c(r) C_L^c(r)}{|\bar{\mathbf{W}}(r)|} \bar{\Omega}_R r^3 \bar{W}_Y(r) dr, \quad (4.17)$$

and the partial derivative of the drag component of the aerodynamic torque with respect to the rotational velocity of the rotor given by:

$$\left. \frac{\partial T_{R:D;Y}(t)}{\partial \Omega_R(t)} \right|_S = -\frac{3}{2} \int_{r_0}^R \rho c(r) C_D(r) |\bar{\mathbf{W}}(r)| r^2 dr - \frac{3}{2} \int_{r_0}^R \frac{\rho c(r) C_D(r)}{|\bar{\mathbf{W}}(r)|} \bar{\Omega}_R^2 r^4 dr. \quad (4.18)$$

The sensitivity of the aerodynamic torque to changes in the rotational velocity is plotted for different operational states in the above rated regime in Figure 4.1.b. It can be observed that it is increasingly negative for increasing wind speeds. This sensitivity has to be negative for the system to be stable, if it would be positive, an acceleration would lead to an increase in aerodynamic torque, which in turn would again cause acceleration, leading to instability.

4.1.3 AERODYNAMIC TORQUE SENSITIVITY TO PITCH ANGLE VARIATIONS

This section presents the sensitivity of the torque to changes in the pitch angle of the blades. Since the only component of the torque depending on the pitch angle is the angle of attack dependent lift component, the sensitivity is defined as follows:

$$\left. \frac{\partial T_{R:A;Y}(t)}{\partial \beta(t)} \right|_S = \left. \frac{\partial T_{R:L;Y}^\alpha(t)}{\partial \beta(t)} \right|_S, \quad (4.19)$$

with:

$$\begin{aligned} \left. \frac{\partial T_{R:L;Y}^\alpha(t)}{\partial \beta(t)} \right|_S &= -\frac{3}{2} \int_{r_0}^R \rho c(r) C_L^\alpha(r) \cos(\beta_0(r) + \bar{\beta}) \bar{\Omega}_R r^2 \bar{W}_Y(r) dr \\ &\quad - \frac{3}{2} \int_{r_0}^R \rho c(r) C_L^\alpha(r) \sin(\beta_0(r) + \bar{\beta}) \{\bar{W}_Y(r)\}^2 r dr. \end{aligned} \quad (4.20)$$

The sensitivity of the aerodynamic torque to changes in the pitch angle of the blades is plotted for different operational states in the above rated regime in Figure 4.1.c. It can be observed that it is increasingly negative for increasing wind speeds, this corresponds to the behavior of the pitch angle as found in Figure 3.4.c, where the needed adjustment of the pitch angle becomes smaller for increasing wind speeds. Obviously, this sensitivity has to be negative for the pitch controller to work, since the torque should decrease for an increase in pitch angle.

4.1.4 AERODYNAMIC TORQUE SENSITIVITY TO INDUCTION VARIATIONS

Lastly, the sensitivity of the aerodynamic torque to changes in the induction factor is presented. As previously done for the other sensitivities, the partial derivate is equal to the sum of the partial derivatives of the different components of the torque:

$$\left. \frac{\partial T_{R;A;Y}(t)}{\partial a(r,t)} \right|_S = \left. \frac{\partial T_{R;L;Y}^\alpha(t)}{\partial a(r,t)} \right|_S + \left. \frac{\partial T_{R;L;Y}^c(t)}{\partial a(r,t)} \right|_S + \left. \frac{\partial T_{R;D;Y}(t)}{\partial a(r,t)} \right|_S, \quad (4.21)$$

where the first partial derivative of the angle of dependent lift component is:

$$\begin{aligned} \left. \frac{\partial T_{R;L;Y}^\alpha(t)}{\partial a(r,t)} \right|_S &= \frac{3}{2} \int_{r_0}^R \rho c(r) C_L^\alpha(r) \sin(\beta_0(r) + \bar{\beta}) \bar{\Omega}_R r^2 \bar{W}_Y^\infty dr \\ &+ \frac{3}{2} \int_{r_0}^R \rho c(r) C_L^\alpha(r) \cos(\beta_0(r) + \bar{\beta}) r \{ \bar{W}_Y^\infty \}^2 (2\bar{a}(r) - 2) dr, \end{aligned} \quad (4.22)$$

the lift component depending on the cambered shape of the airfoils is:

$$\begin{aligned} \left. \frac{\partial T_{R;L;Y}^c(t)}{\partial a(r,t)} \right|_S &= - \frac{3}{2} \int_{r_0}^R \rho c(r) C_L^c(r) |\bar{\mathbf{W}}(r)| r \bar{W}_Y^\infty dr \\ &+ \frac{3}{4} \int_{r_0}^R \frac{\rho c(r) C_L^c(r)}{|\bar{\mathbf{W}}(r)|} \{ \bar{W}_Y^\infty \}^2 (2\bar{a}(r) - 2) \bar{W}_Y(r) r dr, \end{aligned} \quad (4.23)$$

and concluding, the sensitivity of the drag component of the aerodynamic torque to the induction factor is given by:

$$\left. \frac{\partial T_{R;D;Y}(t)}{\partial a(r,t)} \right|_S = - \frac{3}{4} \int_{r_0}^R \frac{\rho c(r) C_D(r)}{|\bar{\mathbf{W}}(r)|} \{ \bar{W}_Y^\infty \}^2 (2\bar{a}(r) - 2) \bar{\Omega}_R r^2 dr \quad (4.24)$$

The sensitivity of the aerodynamic torque to changes in induction factor is plotted for different operational states in the above rated regime in Figure 4.1.a. It can be observed that it is decreasingly negative for increasing wind speeds. This sensitivity is negative because the induced wind speed decreases for an increasing induction factor, resulting in a lower aerodynamic torque.

4.2 NUMERICAL MODEL

The set of differential equations that describe the model and are solved numerically is presented below.

$$\left\{ \begin{array}{l} \Delta \dot{\Omega}_R(t) = \Delta T_{R;A;Y}(\Delta \Omega_R(t), \Delta \beta(t), t) / I_{DT} \\ \Delta \dot{\beta}(t) = K_P N_{GB} \Delta T_{R;A;Y}(\Delta \Omega_R(t), \Delta \beta(t), t) / I_{DT} + K_I N_{GB} \Delta \Omega(t) \\ \dot{\mathbf{a}}(t) = \text{Equation 2.16} \end{array} \right\}$$

The induction is solved for each blade section by using Equation 2.16 and thus it has the same length as the number of blade sections used in the model. Note that the induction factor is only present when the dynamic wake model is used.

4.3 COMPARISON

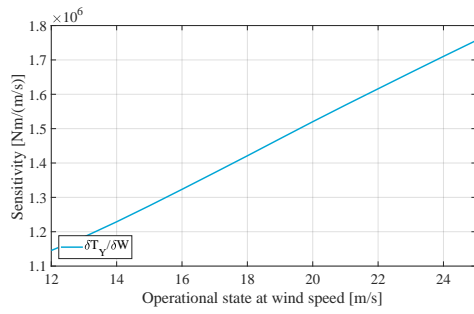
The nonlinear excitation and linearized excitation are compared for a step input wind signal and a turbulent wind signal, this way the effect of the linearization of the aerodynamic excitation and its effects on the behavior of the model is investigated.

4.3.1 STEP WIND INPUT SIGNAL

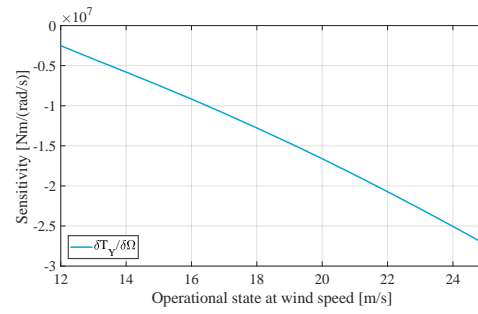
For a step wind input signal (Figure 4.2.a), it can be seen in Figure 4.2.d that the first order Taylor series approximation of the aerodynamic torque acting on the rotor is accurate. However, the pitch angle corresponding to the equilibrium states of the linearized torque is different from the pitch angle corresponding to the equilibrium states of the nonlinear torque (Figure 4.2.c), this difference is more significant for wind velocities higher than the considered mean wind velocity (15 m/s). The small overestimation of the equilibrium pitch angle for wind velocities below the mean velocity, and underestimation for wind speeds above the mean value, result in an over- and underestimation of the thrust force acting on the rotor, as is seen in Figure 4.2.e. The behavior of the rotational velocity (Figure 4.2.b) is accurate since the torque is approximated accurately and the response speed of the blade pitch controller does not deviate significantly for the first two step increases. Higher step increases of the wind velocity will lead to larger deviations in the equilibrium pitch angle since the torque to pitch sensitivity does not increase with wind velocity for the linearized aerodynamic torque model. These larger deviations and underestimated sensitivity will result in higher peaks in the rotational velocity, because more pitching is required in the linearized model than in the nonlinear model to reach equilibrium again. The chosen initial values of the time dependent parameters correspond to the equilibrium state belonging to a wind velocity of 15 m/s, since the wind signal starts at 13 m/s, there is an immediate disturbance of the equilibrium, resulting in the start up behavior seen in Figure 4.2.b to 4.2.e.

4.3.2 TURBULENT WIND INPUT SIGNAL

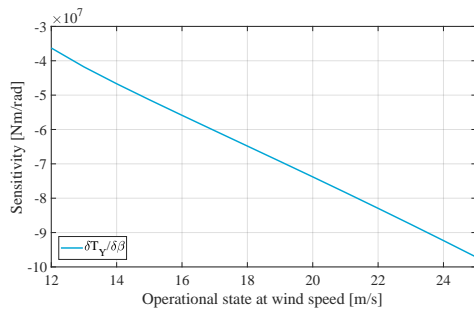
The conclusions drawn in the previous section also apply in the case of a turbulent wind input signal (Figure 4.3.a). Since the signal is mostly above the wind velocity of 15 m/s at which the operational state and thus partial derivatives are defined, the sensitivity of the aerodynamic torque to the pitch angle is underestimated. This underestimation leads to an overestimation of the pitch angle, see Figure 4.3.c, since higher pitch angles are required to compensate for the increase in wind speed. Since the gains of the blade pitch controller are the same for the nonlinear and linearized model, but the torque to pitch sensitivity (for this particular input signal) is underestimated in the linearized model, the peaks in the rotational velocity of the rotor will be higher for the linearized model. In other words, the pitch effectiveness is smaller for the linearized model, which also results in the peaks of the aerodynamic torque being slightly larger, see Figure 4.3.d. Due to the overestimation of the pitch angles, the thrust force will be underestimated. Figure 4.3.e shows this underestimation, note that the difference is the largest for the periods with the highest wind velocities and thus pitch angles. The initial values of the time dependent parameters are corresponding to the operational state belonging to a wind velocity of 15 m/s.



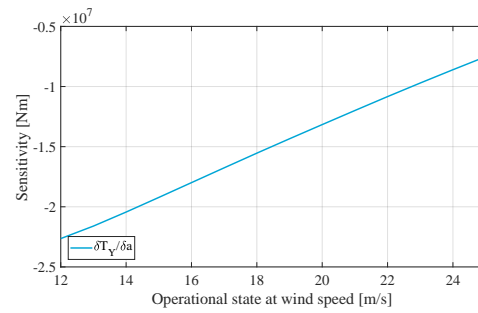
(a)



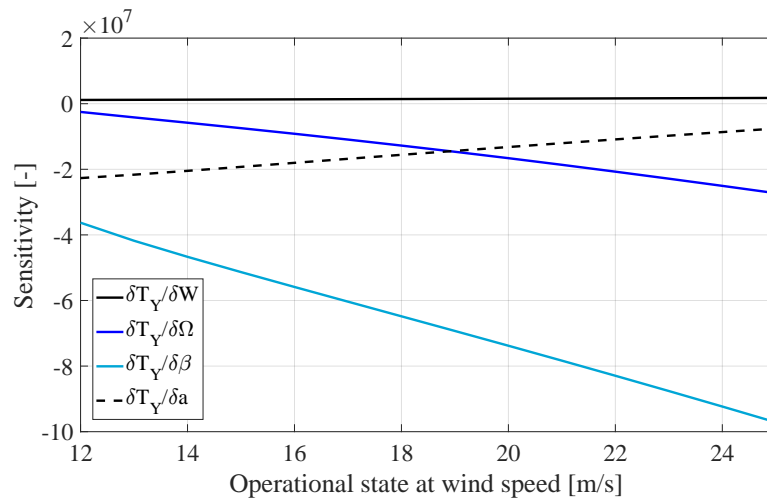
(b)



(c)

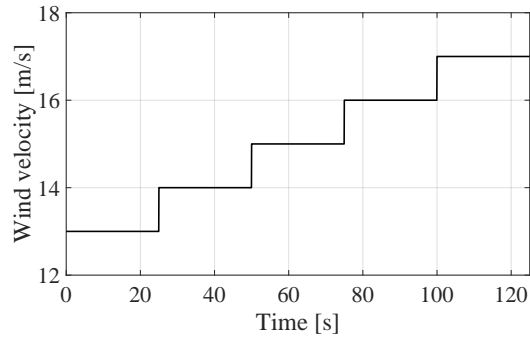


(d)

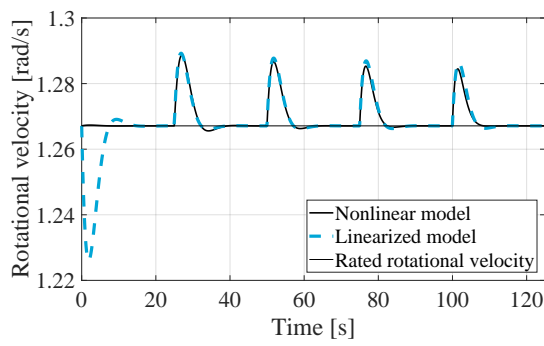


(e)

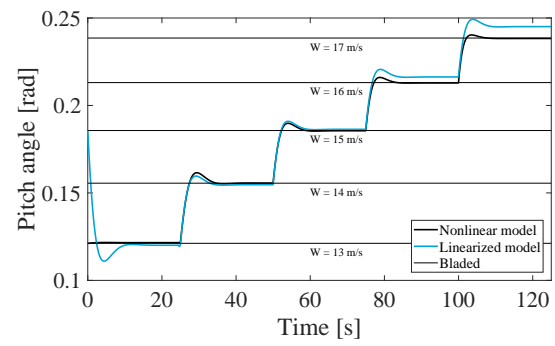
Figure 4.1: The aerodynamic torque sensitivity to wind speed (a), rotational velocity (b), pitch angle (c), induction factor (d) and all (e).



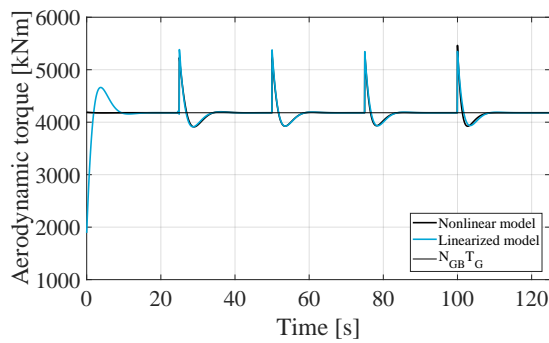
(a)



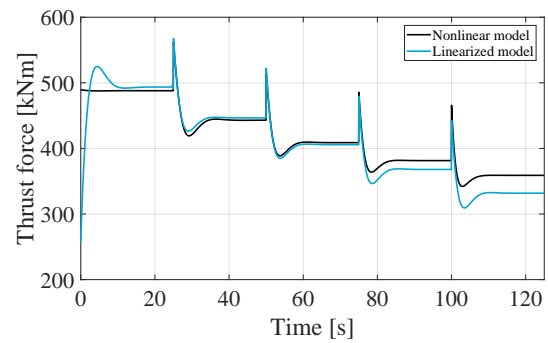
(b)



(c)



(d)



(e)

Figure 4.2: Results for step wind input with wind signal (a), rotational velocity (b), pitch angle (c), torque (d) and thrust force (e) for both the nonlinear and linearized model.

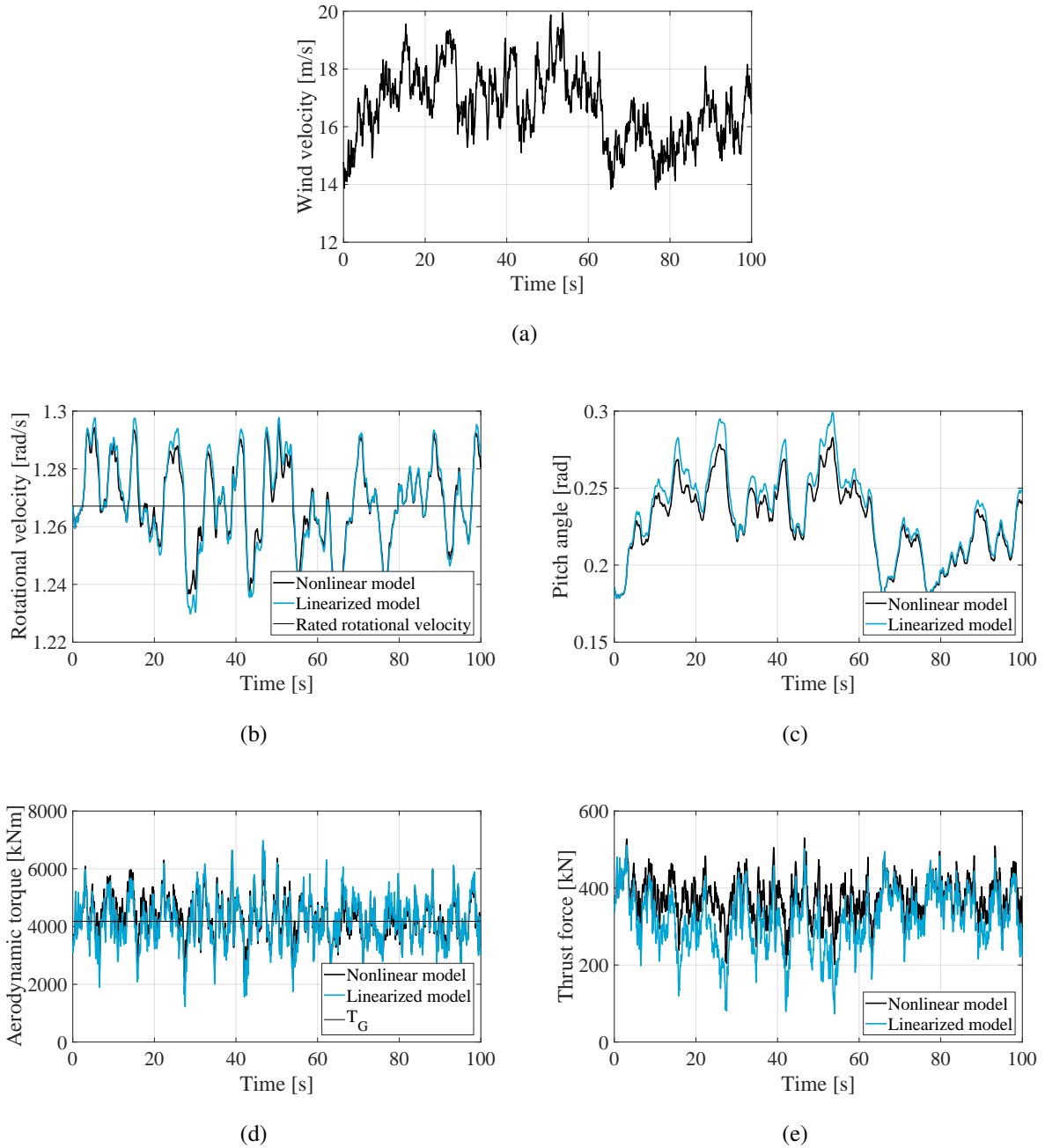


Figure 4.3: Results for turbulent wind input with wind signal (a), rotational velocity (b), pitch angle (c), torque (d) and thrust force (e) for both the nonlinear and linearized model.

5 | WIND TURBINE MODEL WITH NONLINEAR AERODYNAMIC EXCITATION

This chapter describes the model including a monopile support structure and flexible drivetrain shafts while making use of the nonlinear aerodynamic excitation model. Since the stiffness and damping of the drivetrain shafts is included, the two mass model is used.

5.1 EQUATION OF MOTION

The equation of motion of the support structure is based on [10]. The total number of degrees of freedom of the tower model is denoted by n , and is equal to the amount of nodes of the discretized tower model times the six degrees of freedom (translation in the direction of the three axes and rotation around the X, Y, and Z-axis) of each node. The displacement and rotation of the nodes are denoted by the vector $\mathbf{v}(t)$:

$$\mathbf{v}(t) = \begin{bmatrix} \mathbf{u}^1(t) \\ \boldsymbol{\theta}^1(t) \\ \vdots \\ \mathbf{u}^{(n/6)}(t) \\ \boldsymbol{\theta}^{(n/6)}(t) \end{bmatrix}, \quad (5.1)$$

in which $\mathbf{u}^i(t)$ describes the three translations of node i and $\boldsymbol{\theta}^i(t)$ the three rotations. The node numbering starts at the tower top with 1 and the vector describing the displacements and rotations of the tower top can thus be denoted by $\mathbf{v}^1(t)$. The equation of motion of the support structure and rotor-hub-nacelle-unit is defined as follows:

$$\mathbf{M}\ddot{\mathbf{v}}(t) + \mathbf{C}\dot{\mathbf{v}}(t) + \mathbf{K}\mathbf{v}(t) = \mathbf{Q}(t). \quad (5.2)$$

The mass matrix \mathbf{M} consists of a mass matrix describing the tower structure, \mathbf{M}_T , of size $n \times n$, which also includes the nacelle and hub masses, and a mass matrix related to the rotor, \mathbf{M}_R . The rotor mass matrix corresponds to the tower top, and thus to the six degrees of freedom related to the top node, hence its size is 6×6 :

$$\mathbf{M} = \mathbf{M}_T + \begin{bmatrix} \mathbf{M}_R & \mathbf{0}_{6 \times (n-6)} \\ \mathbf{0}_{(n-6) \times 6} & \mathbf{0}_{(n-6) \times (n-6)} \end{bmatrix}, \quad (5.3)$$

where \mathbf{M}_R is defined as:

$$\mathbf{M}_R = \int_{r_0}^R m(r)r \begin{bmatrix} \frac{3}{r} & 0 & 0 & 0 & 0 & 3\frac{d}{r} \\ 0 & \frac{3}{r} & 0 & 0 & 0 & 0 \\ 0 & 0 & \frac{3}{r} & -3\frac{d}{r} & 0 & 0 \\ 0 & 0 & -3\frac{d}{r} & \frac{3}{2}r + 3\frac{d^2}{r} & 0 & 0 \\ 0 & 0 & 0 & 0 & 3r & 0 \\ 3\frac{d}{r} & 0 & 0 & 0 & 0 & \frac{3}{2}r + 3\frac{d^2}{r} \end{bmatrix} dr, \quad (5.4)$$

in which d denotes the distance between the center of rotation of the rotor and the origin of the axis system. Similarly as in the mass matrix, the damping matrix \mathbf{C} also contains a part related to the rotor, \mathbf{C}_R , however, there is no damping included in the model of tower, therefore, the damping matrix mainly consists of zeros:

$$\mathbf{C} = \begin{bmatrix} \mathbf{C}_R & \mathbf{0}_{6 \times (n-6)} \\ \mathbf{0}_{(n-6) \times 6} & \mathbf{0}_{(n-6) \times (n-6)} \end{bmatrix}, \quad (5.5)$$

with \mathbf{C}_R being the following matrix of size 6×6 :

$$\mathbf{C}_R = \int_{r_0}^R m(r)\bar{\Omega}_R r \begin{bmatrix} 0 & 0 & 0 & 0 & 0 & 0 \\ 0 & 0 & 0 & 0 & 0 & 0 \\ 0 & 0 & 0 & 0 & 0 & 0 \\ 0 & 0 & 0 & 0 & 0 & 3r \\ 0 & 0 & 0 & 0 & 0 & 0 \\ 0 & 0 & 0 & -3r & 0 & 0 \end{bmatrix} dr. \quad (5.6)$$

The stiffness matrix \mathbf{K} is equal to the stiffness matrix of the tower, \mathbf{K}_T , of size $n \times n$, since the rotor does not contribute to the stiffness matrix.

$$\mathbf{K} = \mathbf{K}_T \quad (5.7)$$

The forces and moments acting on the nodes are described by the excitation vector $\mathbf{Q}(t)$ of length n . Since only the aerodynamic excitation is included, the only node to which forces and moments are applied is the top node corresponding to the tower top. The aerodynamic excitation acting on the rotor, $\mathbf{Q}_{R:A}(t)$, is defined in [10] and of size 6×1 :

$$\mathbf{Q}_{R:A}(t) = \begin{bmatrix} F_{R:A:X}(t) \\ F_{R:A:Y}(t) \\ F_{R:A:Z}(t) \\ T_{R:A:X}(t) \\ T_{R:A:Y}(t) \\ T_{R:A:Z}(t) \end{bmatrix}, \quad (5.8)$$

it contains the forces and moments acting on the rotor. The loads acting on the tower top are transferred from the rotor and thus equal, with exception of the moment around the Y-axis. The moment around the Y-axis acting on the tower top is approximated as the aerodynamic torque acting on the rotor minus the inertial torques of the rotor and generator, as described in Equation 5.9. This method is based on the d'Alembert principle which is valid for one degree of freedom systems, and not for two degree of freedom systems, hence this being an approximation.

$$\mathbf{Q}(t) = \begin{bmatrix} \mathbf{Q}_{R:A}(t) \\ \mathbf{0}_{(n-6) \times 1} \end{bmatrix} - \begin{bmatrix} \mathbf{0}_{4 \times 1} \\ I_R \Delta \dot{\Omega}_R(t) + I_G \Delta \dot{\Omega}_G(t) \\ \mathbf{0}_{(n-5) \times 1} \end{bmatrix} \quad (5.9)$$

To the system of equations describing the motions of the tower structure, the equation of motion of the flexible drivetrain, as defined in Section 2.4.2, is added:

$$\begin{bmatrix} I_R & 0 \\ 0 & I_G \end{bmatrix} \begin{bmatrix} \dot{\Omega}_R(t) \\ \dot{\Omega}_G(t) \end{bmatrix} + C_{DT} \begin{bmatrix} 1 & \frac{-1}{N_{GB}} \\ \frac{-1}{N_{GB}} & \frac{1}{N_{GB}^2} \end{bmatrix} \begin{bmatrix} \Omega_R(t) \\ \Omega_G(t) \end{bmatrix} + K_{DT} \begin{bmatrix} 1 & \frac{-1}{N_{GB}} \\ \frac{-1}{N_{GB}} & \frac{1}{N_{GB}^2} \end{bmatrix} \begin{bmatrix} \int_0^t \Omega_R(t) dt \\ \int_0^t \Omega_G(t) dt \end{bmatrix} = \begin{bmatrix} T_{R:A;Y}(t) \\ -T_G \end{bmatrix}. \quad (5.10)$$

5.2 NUMERICAL MODEL

To decrease the number of differential equations that need to be solved, modal reduction is applied to Equation 5.2. In modal analysis the motions are approximated by a superposition of the multiplication of a certain amount of normal modes and unknown functions of time. If only the normal modes with the lowest frequencies are considered, the dimensions of the model that need to be solved can be reduced drastically, thus reducing computational expense. The initial vector $\mathbf{v}(t)$ containing the degrees of freedom, is replaced by $\mathbf{E}\mathbf{w}(t)$, where \mathbf{E} contains the eigen vectors describing the considered mode shapes and $\mathbf{w}(t)$ are new unknown functions of time. After finding the solution for $\mathbf{w}(t)$, it is transferred back to the initial vector $\mathbf{v}(t)$. The following set of equations is solved numerically in Matlab and the results are discussed in the following section.

$$\left\{ \begin{array}{l} \ddot{\mathbf{w}}(t) = \left(\mathbf{E}^T \mathbf{M} \mathbf{E} \right)^{-1} \left(\mathbf{E}^T \mathbf{Q}(t) - \mathbf{E}^T \mathbf{C} \mathbf{E} \dot{\mathbf{w}}(t) - \mathbf{E}^T \mathbf{K} \mathbf{E} \mathbf{w}(t) \right) \\ \Delta \dot{\Omega}_R(t) = T_{R:A;Y}(t) - C_{DT} \left(\Delta \Omega_R(t) - \frac{1}{N_{GB}} \Delta \Omega_G(t) \right) - K_{DT} \left(\int_0^t \Delta \Omega_R(t) dt - \frac{1}{N_{GB}} \int_0^t \Delta \Omega_G(t) dt \right) \\ \Delta \dot{\Omega}_G(t) = -T_G - C_{DT} \left(\frac{1}{N_{GB}^2} \Delta \Omega_G(t) - \frac{1}{N_{GB}} \Delta \Omega_R(t) \right) - K_{DT} \left(\frac{1}{N_{GB}^2} \int_0^t \Delta \Omega_G(t) dt - \frac{1}{N_{GB}} \int_0^t \Delta \Omega_R(t) dt \right) \\ \Delta \dot{\beta}(t) = K_P \left(-T_G - C_{DT} \left(\frac{1}{N_{GB}^2} \Delta \Omega_G(t) - \frac{1}{N_{GB}} \Delta \Omega_R(t) \right) - K_{DT} \left(\frac{1}{N_{GB}^2} \int_0^t \Delta \Omega_G(t) dt - \frac{1}{N_{GB}} \int_0^t \Delta \Omega_R(t) dt \right) \right) \\ \quad + K_I \Delta \Omega_G(t) \\ \dot{\mathbf{a}}(t) = \text{Equation 2.16} \end{array} \right.$$

5.3 VALIDATION

Similarly to Chapter 3, a validation of the model is done by comparing its results to the commercial wind turbine simulation software Bladed. Including a support structure, and thus allowing the rotor to move in space, complicates the model since now the motion of the rotor has an effect on the aerodynamic excitation applied to the rotor, which in turn affects the motion. The model is compared to Bladed results for both a step input and a turbulent input. For both the model and Bladed, only the first two modes of the support structure are used, which contain the fore-aft and side-to-side motions. Both simulations use the static displacement related to the mean operational state S as the initial condition for the support structure displacement. All other initial values of the time dependent parameters also correspond to state S , which is evaluated for a wind velocity of 15 m/s. Differences in initial conditions between the model and Bladed are observed.

5.3.1 STEP WIND INPUT SIGNAL

The step wind input signal used is presented in Figure 5.1.a, where the first ten seconds the wind velocity is 15 m/s, after which it increases stepwise to 16 m/s. In Figure 5.1.d the pitch angle is presented, it can be seen that although both the model and Bladed start at the same pitch angle, Bladed converges to another equilibrium for the 15 m/s wind speed, which in turn also affects the behavior of the rotational velocity at the start of the simulation. Based on this unexplained behavior a difference in results between the model and Bladed will be

inevitable. The slow convergence of the pitch angle of the model to the new equilibrium pitch angle belonging to 16 m/s is caused by the use of the dynamic wake model. The fore-aft displacement (Figure 5.1.b) decreases after the increase in wind velocity, due to the pitch angle becoming larger, which results in a reduced thrust force, see Figure 5.1.f. The aerodynamic torque (Figure 5.1.e) shows a spike at the step increase of the wind velocity, as expected. Due to the pitch control system the torque converges back to the equilibrium position, where the torque is equal to the equivalent electromagnetic generator torque.

5.3.2 TURBULENT WIND INPUT SIGNAL

The same turbulent wind signal is used as in previous chapters, see Figure 5.2.a. The match between the rotational velocity and pitch angle is very satisfying, as can be observed in Figure 5.2.b and 5.2.c, respectively. The smaller peaks in the pitch angle of the model result in a less fluctuating thrust force, see Figure 5.2.e, where the differences are largest at the moments where the largest difference in pitch angle occurs. Figure 5.3 shows the side-to-side and fore-aft motions of the tower top. A discrete Fourier transform is applied to these displacements which results in the corresponding spectra of the frequency content. It can be seen that the peaks of the spectra are the same for both the model and Bladed, these peaks correspond to the eigen frequencies of the mode shapes.

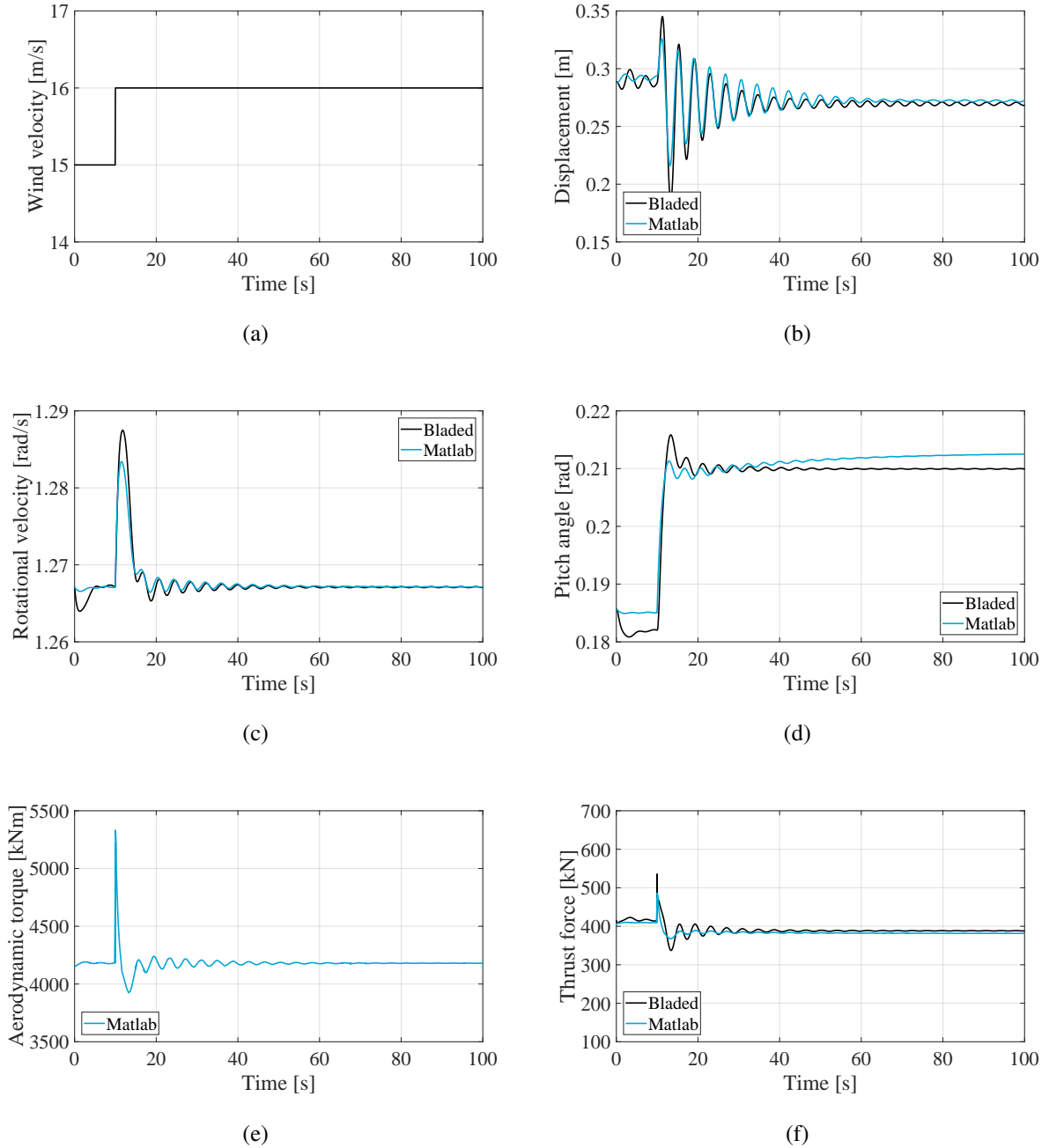


Figure 5.1: Results for step wind input with wind signal (a), fore-aft motion $u_Y^1(t)$ (b), rotational velocity (c), pitch angle (d), aerodynamic torque (e) and thrust force (f) for both the nonlinear model and Bladed.

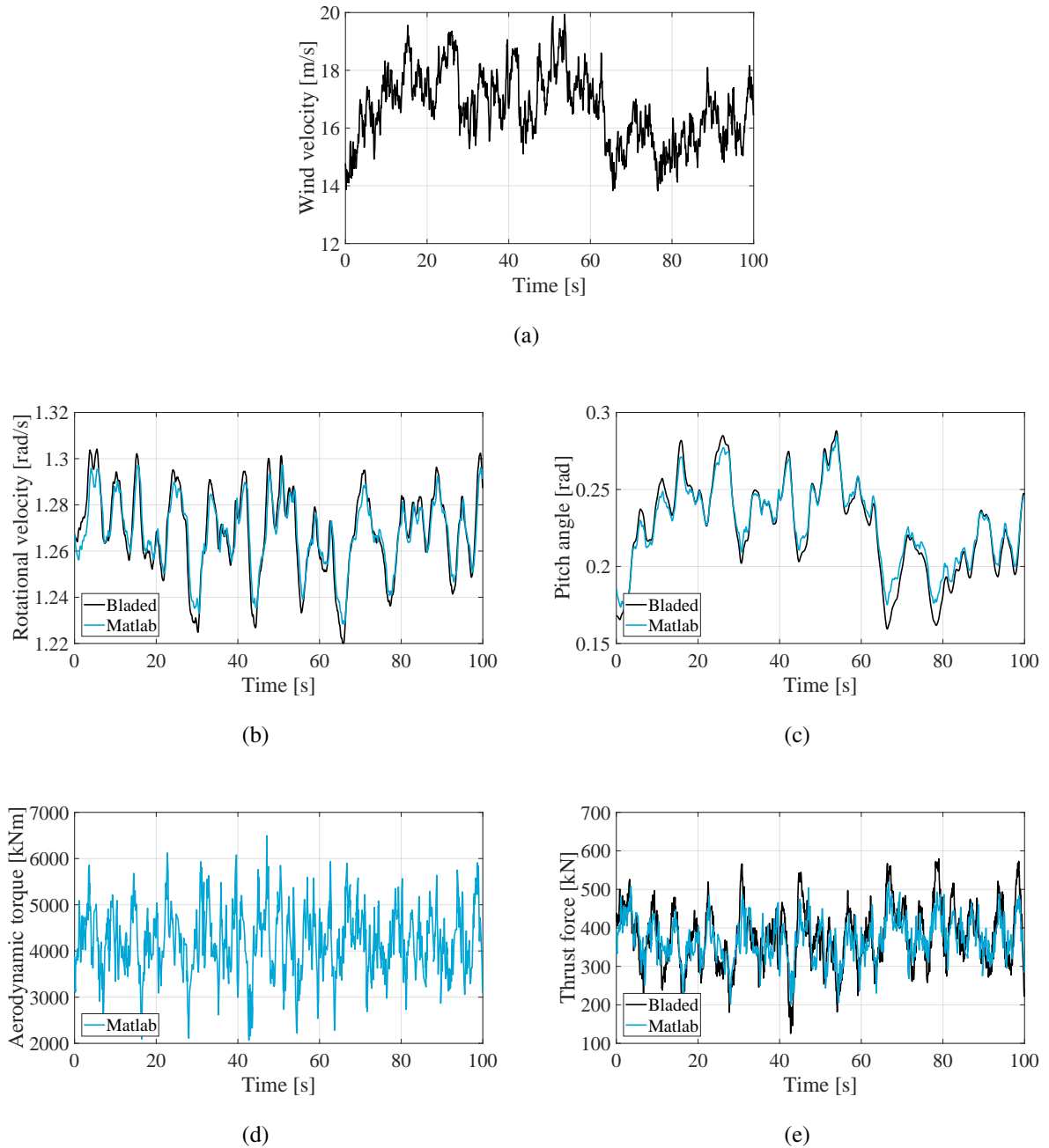
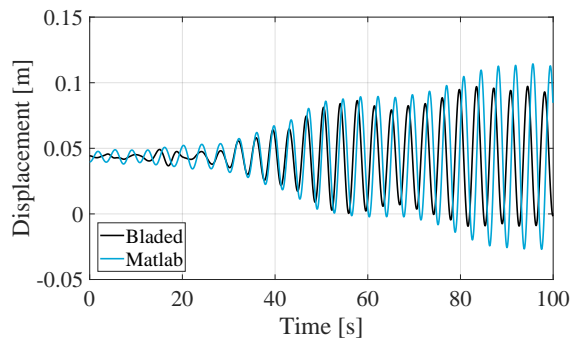
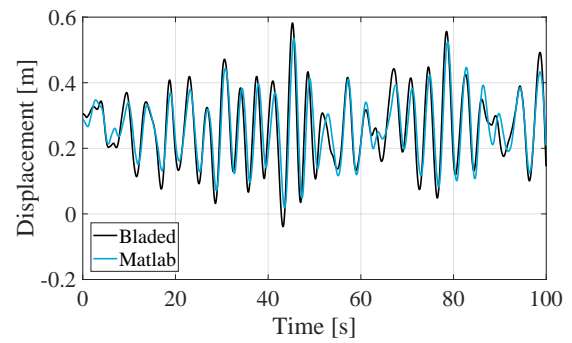


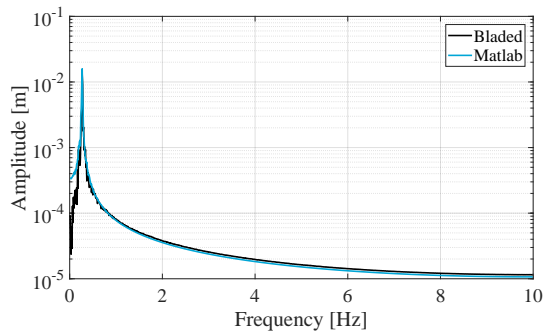
Figure 5.2: Results for turbulent wind input with wind signal (a), rotational velocity (b), pitch angle (c), aerodynamic torque (d) and thrust force (e) for both the nonlinear model and Bladed.



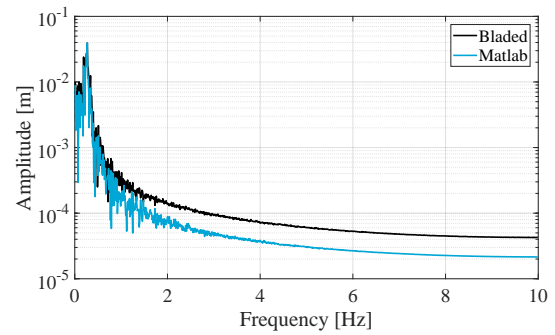
(a)



(b)



(c)



(d)

Figure 5.3: Side-to-side displacement of the tower top $u_x^1(t)$ (a), fore-aft motion of the tower top $u_y^1(t)$ (b), the side-to-side motion of the tower top in the frequency domain (c) and the fore-aft displacement in the frequency domain (d).

6 | WIND TURBINE MODEL WITH LINEARIZED AERODYNAMIC EXCITATION

This chapter describes a model in which the aerodynamic excitation is linearized with respect to the wind velocity, structural motions, rotational rotor velocity, pitch angle and induction factor. The partial derivatives with respect to the wind velocity and structural motions are based on [10]. Whereas Chapter 4 only describes the linearization of the aerodynamic torque, this chapter presents all three aerodynamic forces and moments acting on the rotor while the same approach is used. A first order Taylor series expansion is applied to the aerodynamic excitation to linearize the excitation with respect to the wind velocity, structural motions, rotational rotor velocity, pitch angle and induction factor. The mean excitation and partial derivatives are presented in the following sections.

$$\begin{aligned} \mathbf{Q}_{R:A}(t) \approx \bar{\mathbf{Q}}_{R:A} \Big|_S + \frac{\partial \mathbf{Q}_{R:A}(t)}{\partial W_Y(r,t)} \Big|_S \Delta W_Y(r,t) + \frac{\partial \mathbf{Q}_{R:A}(t)}{\partial \mathbf{v}^1(t)} \Big|_S \mathbf{v}^1(t) + \frac{\partial \mathbf{Q}_{R:A}(t)}{\partial \dot{\mathbf{v}}^1(t)} \Big|_S \dot{\mathbf{v}}^1(t) + \frac{\partial \mathbf{Q}_{R:A}(t)}{\partial \ddot{\mathbf{v}}^1(t)} \Big|_S \ddot{\mathbf{v}}^1(t) \\ + \frac{\partial \mathbf{Q}_{R:A}(t)}{\partial \Omega_R(t)} \Big|_S \Delta \Omega_R(t) + \frac{\partial \mathbf{Q}_{R:A}(t)}{\partial \beta(t)} \Big|_S \Delta \beta(t) + \frac{\partial \mathbf{Q}_{R:A}(t)}{\partial a(r,t)} \Big|_S \Delta a(r,t) \end{aligned} \quad (6.1)$$

The aerodynamic force is separated in a lift force caused by the angle of attack between the wind and the blades, $\mathbf{Q}_{R:L}^a(t)$, a lift force caused by the camber of the airfoils, $\mathbf{Q}_{R:L}^c(t)$, a drag force, $\mathbf{Q}_{R:D}(t)$, and an inertia force, $\mathbf{Q}_{R:I}(t)$. The mean force components and partial derivatives are evaluated at the operating point S . In this case the displacements and rotations and the corresponding velocities and accelerations of the support structure are added to the definition of the state:

$$S = \left\{ W_Y(r,t) = \bar{W}_Y(r), \mathbf{v}^1(t) = 0, \dot{\mathbf{v}}^1(t) = 0, \ddot{\mathbf{v}}^1(t) = 0, \Omega_R(t) = \bar{\Omega}_R, \beta(t) = \bar{\beta}, a(r,t) = \bar{a}(r) \right\}. \quad (6.2)$$

Where the induction factors are evaluated at the wind velocity corresponding to operational point S . The mean of the displacement and rotation is assumed to be zero to decrease the number of terms, this has no significant effect on the interaction [10]. The following sections describe the mean component and the various sensitivities of the first order Taylor series approximation of the aerodynamic excitation as presented in Equation 6.1.

6.1 MEAN AERODYNAMIC EXCITATION

The mean aerodynamic excitation acting on the rotor is divided into three parts, related to the lift, drag and inertia:

$$\bar{\mathbf{Q}}_{R:A} \Big|_S = \bar{\mathbf{Q}}_{R:L}^\alpha \Big|_S + \bar{\mathbf{Q}}_{R:L}^c \Big|_S + \bar{\mathbf{Q}}_{R:D} \Big|_S + \bar{\mathbf{Q}}_{R:I} \Big|_S, \quad (6.3)$$

where the lift component depending on the angle of attack is defined as:

$$\begin{aligned} \bar{\mathbf{Q}}_{R:L}^\alpha \Big|_S &= \frac{3}{2} \int_{r_0}^R \rho c(r) C_L^\alpha(r) \sin(\beta_0(r) + \bar{\beta}) [0 \quad -\bar{\Omega}_R^2 r^2 \quad 0 \quad 0 \quad -\bar{\Omega}_R r^2 \bar{W}_Y(r) \quad 0]^T dr \\ &+ \frac{3}{2} \int_{r_0}^R \rho c(r) C_L^\alpha(r) \cos(\beta_0(r) + \bar{\beta}) [0 \quad \bar{\Omega}_R r \bar{W}_Y(r) \quad 0 \quad 0 \quad \{\bar{W}_Y(r)\}^2 r \quad 0]^T dr. \end{aligned} \quad (6.4)$$

The mean excitation component due to the cambered shape of the airfoils is

$$\bar{\mathbf{Q}}_{R:L}^c \Big|_S = \frac{3}{2} \int_{r_0}^R \rho c(r) C_L^c(r) |\bar{\mathbf{W}}(r)| [0 \quad \bar{\Omega}_R r \quad 0 \quad 0 \quad \bar{W}_Y(r) r \quad 0]^T dr, \quad (6.5)$$

and the drag part is defined as

$$\bar{\mathbf{Q}}_{R:D} \Big|_S = \frac{3}{2} \int_{r_0}^R \rho c(r) C_D(r) |\bar{\mathbf{W}}(r)| [0 \quad \bar{W}_Y(r) \quad 0 \quad 0 \quad -\bar{\Omega}_R r^2 \quad 0]^T dr. \quad (6.6)$$

The mean component of the inertia related component is zero:

$$\bar{\mathbf{Q}}_{R:I} = \mathbf{0}_{6 \times 1}, \quad (6.7)$$

and the relative velocity is defined as:

$$|\bar{\mathbf{W}}(r)| = \sqrt{(\bar{\Omega}_R r)^2 + \{\bar{W}_Y(r)\}^2}. \quad (6.8)$$

6.2 AERODYNAMIC EXCITATION SENSITIVITIES

In this section the partial derivatives of the aerodynamic excitation with respect to the wind velocity, structural motions, rotational rotor velocity, pitch angle and induction factor are presented.

6.2.1 AERODYNAMIC EXCITATION SENSITIVITY TO WIND SPEED VARIATIONS

The sensitivity of the aerodynamic excitation to changes in the wind speed at a certain state S is defined as the sum of the partial derivatives of the different components of the excitation:

$$\frac{\partial \mathbf{Q}_{R:A}(t)}{\partial W_Y(r, t)} \Big|_S = \frac{\partial \mathbf{Q}_{R:L}^\alpha(t)}{\partial W_Y(r, t)} \Big|_S + \frac{\partial \mathbf{Q}_{R:L}^c(t)}{\partial W_Y(r, t)} \Big|_S + \frac{\partial \mathbf{Q}_{R:D}(t)}{\partial W_Y(r, t)} \Big|_S + \frac{\partial \mathbf{Q}_{R:I}(t)}{\partial W_Y(r, t)} \Big|_S, \quad (6.9)$$

where the angle of attack dependent lift component is defined as:

$$\begin{aligned} \frac{\partial \mathbf{Q}_{R:L}^\alpha(t)}{\partial W_Y(r, t)} \Big|_S &= \frac{3}{2} \int_{r_0}^R \rho c(r) C_L^\alpha(r) \sin(\beta_0(r) + \bar{\beta}) [0 \quad 0 \quad 0 \quad 0 \quad -\bar{\Omega}_R r^2 \quad 0]^T dr \\ &+ \frac{3}{2} \int_{r_0}^R \rho c(r) C_L^\alpha(r) \cos(\beta_0(r) + \bar{\beta}) [0 \quad \bar{\Omega}_R r \quad 0 \quad 0 \quad 2\bar{W}_Y(r) r \quad 0]^T dr, \end{aligned} \quad (6.10)$$

and the component depending on the camber of the airfoils is defined as follows:

$$\begin{aligned} \left. \frac{\partial \mathbf{Q}_{R:L}^c(t)}{\partial W_Y(r, t)} \right|_S &= \frac{3}{2} \int_{r_0}^R \rho c(r) C_L^c(r) |\bar{\mathbf{W}}(r)| [0 \ 0 \ 0 \ 0 \ r \ 0]^T dr \\ &+ \frac{3}{2} \int_{r_0}^R \frac{\rho c(r) C_L^c(r)}{|\bar{\mathbf{W}}(r)|} [0 \ \bar{\Omega}_R r \bar{W}_Y(t) \ 0 \ 0 \ \{\bar{W}_Y(t)\}^2 r \ 0]^T dr. \end{aligned} \quad (6.11)$$

The drag related part of the aerodynamic excitation sensitivity to changes in the wind velocity is presented in Equation 6.12:

$$\begin{aligned} \left. \frac{\partial \mathbf{Q}_{R:D}(t)}{\partial W_Y(r, t)} \right|_S &= \frac{3}{2} \int_{r_0}^R \rho c(r) C_D(r) |\bar{\mathbf{W}}(r)| [0 \ 1 \ 0 \ 0 \ 0 \ 0]^T dr \\ &+ \frac{3}{2} \int_{r_0}^R \frac{\rho c(r) C_D(r, W_Y)}{|\bar{\mathbf{W}}(r)|} [0 \ \{\bar{W}_Y(t)\}^2 \ 0 \ 0 \ -\bar{\Omega}_R^2 r^2 \bar{W}_Y(t) \ 0]^T dr. \end{aligned} \quad (6.12)$$

And finally, the inertia term equals zero:

$$\left. \frac{\partial \mathbf{Q}_{R:I}(t)}{\partial W_Y(t)} \right|_S = \mathbf{0}_{6 \times 1}. \quad (6.13)$$

6.2.2 AERODYNAMIC EXCITATION SENSITIVITY TO STRUCTURAL ROTATION

This section presents the sensitivity of the aerodynamic excitation to changes in the structural rotation of the tower top. The aerodynamic excitation does not change due to structural displacements, hence the first three columns of the following matrices being zero.

$$\left. \frac{\partial \mathbf{Q}(t)}{\partial \mathbf{v}^1(t)} \right|_S = \left. \frac{\partial \mathbf{Q}_{R:L}^\alpha(t)}{\partial \mathbf{v}^1(t)} \right|_S + \left. \frac{\partial \mathbf{Q}_{R:L}^c(t)}{\partial \mathbf{v}^1(t)} \right|_S + \left. \frac{\partial \mathbf{Q}_{R:D}(t)}{\partial \mathbf{v}^1(t)} \right|_S + \left. \frac{\partial \mathbf{Q}_{R:I}(t)}{\partial \mathbf{v}^1(t)} \right|_S \quad (6.14)$$

The angle of attack dependent lift component of the aerodynamic excitation sensitivity to structural rotation is given in Equation 6.15:

$$\begin{aligned} \left. \frac{\partial \mathbf{Q}_{R:L}^\alpha(t)}{\partial \mathbf{v}^1(t)} \right|_S &= \frac{3}{2} \int_{r_0}^R \rho c(r) C_L^\alpha(r) \sin(\beta_0(r) + \bar{\beta}) \begin{bmatrix} 0 & 0 & 0 & 0 & 0 & \left(\frac{\bar{\Omega}_R^2 r^2}{+\frac{1}{2} \{\bar{W}_Y(r)\}^2} \right) \\ 0 & 0 & 0 & 0 & 0 & 0 \\ 0 & 0 & 0 & \left(\frac{-\bar{\Omega}_R^2 r^2}{-\frac{1}{2} \{\bar{W}_Y(r)\}^2} \right) & 0 & 0 \\ 0 & 0 & 0 & \frac{1}{2} \{\bar{W}_Y(r)\}^2 d & 0 & 0 \\ 0 & 0 & 0 & 0 & 0 & 0 \\ 0 & 0 & 0 & 0 & 0 & \frac{1}{2} \{\bar{W}_Y(r)\}^2 d \end{bmatrix} dr \\ &+ \frac{3}{2} \int_{r_0}^R \rho c(r) C_L^\alpha(r) \cos(\beta_0(r) + \bar{\beta}) \begin{bmatrix} 0 & 0 & 0 & 0 & 0 & -\bar{W}_Y(r) \bar{\Omega}_R r \\ 0 & 0 & 0 & 0 & 0 & 0 \\ 0 & 0 & 0 & \bar{W}_Y(r) \bar{\Omega}_R r & 0 & 0 \\ 0 & 0 & 0 & 0 & 0 & -\frac{1}{2} \{\bar{W}_Y(r)\}^2 r \\ 0 & 0 & 0 & 0 & 0 & 0 \\ 0 & 0 & 0 & \frac{1}{2} \{\bar{W}_Y(r)\}^2 r & 0 & 0 \end{bmatrix} dr. \end{aligned} \quad (6.15)$$

The partial derivative of the cambered lift part of the aerodynamic excitation with respect to the structural displacements and rotations is:

$$\begin{aligned} \left. \frac{\partial \mathbf{Q}_{R:L}^c(t)}{\partial \mathbf{v}^1(t)} \right|_S &= \frac{3}{2} \int_{r_0}^R \rho c(r) C_L^c(r) |\bar{\mathbf{W}}(r)| \begin{bmatrix} 0 & 0 & 0 & 0 & 0 & -\bar{\Omega}_R r \\ 0 & 0 & 0 & 0 & 0 & 0 \\ 0 & 0 & 0 & \bar{\Omega}_R r & 0 & 0 \\ 0 & 0 & 0 & 0 & 0 & 0 \\ 0 & 0 & 0 & 0 & 0 & 0 \\ 0 & 0 & 0 & 0 & 0 & 0 \end{bmatrix} dr \\ &+ \frac{3}{2} \int_{r_0}^R \frac{\rho c(r) C_L^c(r)}{|\bar{\mathbf{W}}(r)|} \begin{bmatrix} 0 & 0 & 0 & 0 & 0 & -\bar{\Omega}_R r \{\bar{W}_Y(r)\}^2 \\ 0 & 0 & 0 & 0 & 0 & 0 \\ 0 & 0 & 0 & \bar{\Omega}_R r \{\bar{W}_Y(r)\}^2 & 0 & 0 \\ 0 & 0 & 0 & -\frac{1}{2} \bar{\Omega}_R r \{\bar{W}_Y(r)\}^2 d & 0 & -\frac{1}{2} \{\bar{W}_Y(r)\}^3 r \\ 0 & 0 & 0 & 0 & 0 & 0 \\ 0 & 0 & 0 & \frac{1}{2} \{\bar{W}_Y(r)\}^3 r & 0 & -\frac{1}{2} \bar{\Omega}_R r \{\bar{W}_Y(r)\}^2 d \end{bmatrix} dr, \end{aligned} \quad (6.16)$$

while the drag related part is given by:

$$\begin{aligned} \left. \frac{\partial \mathbf{Q}_{R:D}(t)}{\partial \mathbf{v}^1(t)} \right|_S &= \frac{3}{2} \int_{r_0}^R \rho c(r) C_D(r) |\bar{\mathbf{W}}(r)| \begin{bmatrix} 0 & 0 & 0 & 0 & 0 & 0 \\ 0 & 0 & 0 & 0 & 0 & 0 \\ 0 & 0 & 0 & 0 & 0 & 0 \\ 0 & 0 & 0 & \frac{1}{2} \bar{W}_Y(r) d & 0 & \bar{\Omega}_R r^2 \\ 0 & 0 & 0 & 0 & 0 & 0 \\ 0 & 0 & 0 & -\bar{\Omega}_R r^2 & 0 & \frac{1}{2} \bar{W}_Y(r) d \end{bmatrix} dr \\ &+ \frac{3}{2} \int_{r_0}^R \frac{\rho c(r) C_D(r)}{|\bar{\mathbf{W}}(r)|} \begin{bmatrix} 0 & 0 & 0 & 0 & 0 & -\frac{1}{2} \{\bar{W}_Y(r)\}^3 \\ 0 & 0 & 0 & 0 & 0 & 0 \\ 0 & 0 & 0 & \frac{1}{2} \{\bar{W}_Y(r)\}^3 & 0 & 0 \\ 0 & 0 & 0 & \frac{1}{2} \bar{\Omega}_R^2 r^2 \bar{W}_Y(r) d & 0 & \frac{1}{2} \bar{\Omega}_R r^2 \{\bar{W}_Y(r)\}^2 \\ 0 & 0 & 0 & 0 & 0 & 0 \\ 0 & 0 & 0 & -\frac{1}{2} \bar{\Omega}_R r^2 \{\bar{W}_Y(r)\}^2 & 0 & \frac{1}{2} \bar{\Omega}_R^2 r^2 \bar{W}_Y(r) d \end{bmatrix} dr. \end{aligned} \quad (6.17)$$

Lastly, the partial derivate of the inertia component of the aerodynamic excitation with respect to the structural displacement and rotation is presented below:

$$\left. \frac{\partial \mathbf{Q}_{R:I}(t)}{\partial \mathbf{v}^1(t)} \right|_S = \frac{3}{2} \int_{r_0}^R \rho \pi c(r)^2 \begin{bmatrix} 0 & 0 & 0 & \bar{W}_Y(r) \bar{\Omega}_R & 0 & 0 \\ 0 & 0 & 0 & 0 & 0 & 0 \\ 0 & 0 & 0 & 0 & 0 & \bar{W}_Y(r) \bar{\Omega}_R \\ 0 & 0 & 0 & 0 & 0 & -\bar{W}_Y(r) \bar{\Omega}_R d \\ 0 & 0 & 0 & 0 & 0 & 0 \\ 0 & 0 & 0 & \bar{W}_Y(r) \bar{\Omega}_R d & 0 & 0 \end{bmatrix} dr. \quad (6.18)$$

6.2.3 AERODYNAMIC EXCITATION SENSITIVITY TO STRUCTURAL VELOCITY

The aerodynamic excitation is dependent on the structural velocity of the rotor, and therefore, tower top. The partial derivative of the aerodynamic excitation to the structural velocity is divided into four components which are presented below:

$$\left. \frac{\partial \mathbf{Q}_{R:A}(t)}{\partial \dot{\mathbf{v}}^1(t)} \right|_S = \left. \frac{\partial \mathbf{Q}_{R:L}^a(t)}{\partial \dot{\mathbf{v}}^1(t)} \right|_S + \left. \frac{\partial \mathbf{Q}_{R:L}^c(t)}{\partial \dot{\mathbf{v}}^1(t)} \right|_S + \left. \frac{\partial \mathbf{Q}_{R:D}(t)}{\partial \dot{\mathbf{v}}^1(t)} \right|_S + \left. \frac{\partial \mathbf{Q}_{R:I}(t)}{\partial \dot{\mathbf{v}}^1(t)} \right|_S. \quad (6.19)$$

The first component, related to the excitation due to the lift forces depending on the angle of attack, is found to be:

$$\begin{aligned} \frac{\partial \mathbf{Q}_{R:L}^{\alpha}(t)}{\partial \dot{\mathbf{v}}^1(t)} \Big|_S = & \\ & \frac{3}{2} \int_{r_0}^R \rho c(r) C_L^{\alpha}(r) \sin(\beta_0(r) + \bar{\beta}) \begin{bmatrix} -\frac{1}{2} \bar{W}_Y(t) & 0 & 0 & -\frac{1}{2} \bar{\Omega}_R r^2 & 0 & -\frac{1}{2} \bar{W}_Y(r) d \\ 0 & 0 & 0 & 0 & -2 \bar{\Omega}_R r^2 & 0 \\ 0 & 0 & -\frac{1}{2} \bar{W}_Y(r) & \frac{1}{2} \bar{W}_Y(r) d & 0 & -\frac{1}{2} \bar{\Omega}_R r^2 \\ \bar{\Omega}_R r^2 & 0 & \frac{1}{2} \bar{W}_Y(r) d & -\frac{1}{2} \bar{W}_Y(r) d^2 & 0 & \frac{3}{2} \bar{\Omega}_R r^2 d \\ 0 & \bar{\Omega}_R r^2 & 0 & 0 & -r^2 \bar{W}_Y(r) & 0 \\ -\frac{1}{2} \bar{W}_Y(r) d & 0 & \bar{\Omega}_R r^2 & -\frac{3}{2} \bar{\Omega}_R r^2 d & 0 & -\frac{1}{2} \bar{W}_Y(r) d^2 \end{bmatrix} dr \\ & + \frac{3}{2} \int_{r_0}^R \rho c(r) C_L^{\alpha}(r) \cos(\beta_0(r) + \bar{\beta}) \begin{bmatrix} 0 & 0 & 0 & r \bar{W}_Y(r) & 0 & 0 \\ 0 & -\bar{\Omega}_R r & 0 & 0 & r \bar{W}_Y(r) & 0 \\ 0 & 0 & 0 & 0 & 0 & r \bar{W}_Y(r) \\ -\frac{1}{2} r \bar{W}_Y(r) & 0 & 0 & -\frac{1}{2} \bar{\Omega}_R r^3 & 0 & -\frac{3}{2} r \bar{W}_Y(r) d \\ 0 & 0 & 0 & \frac{1}{2} \{ \bar{W}_Y(r) \}^2 r & 0 & 0 \\ 0 & 0 & -\frac{1}{2} r \bar{W}_Y(r) & \frac{3}{2} r \bar{W}_Y(r) d & 0 & -\frac{1}{2} \bar{\Omega}_R r^3 \end{bmatrix} dr, \end{aligned} \quad (6.20)$$

where the second component, related to the camber of the airfoils, is equal to:

$$\begin{aligned} \frac{\partial \mathbf{Q}_{R:L}^c(t)}{\partial \dot{\mathbf{v}}^1(t)} \Big|_S = & \\ & \frac{3}{2} \int_{r_0}^R \rho c(r) C_L^c(r) | \bar{\mathbf{W}}(r) | \begin{bmatrix} 0 & 0 & 0 & \frac{1}{2} r & 0 & 0 \\ 0 & 0 & 0 & 0 & r & 0 \\ 0 & 0 & 0 & 0 & 0 & \frac{1}{2} r \\ -\frac{1}{2} r & 0 & 0 & 0 & 0 & -\frac{3}{2} r d \\ 0 & -r & 0 & 0 & 0 & 0 \\ 0 & 0 & -\frac{1}{2} r & \frac{3}{2} r d & 0 & 0 \end{bmatrix} dr \\ & + \frac{3}{2} \int_{r_0}^R \frac{\rho c(r) C_L^c(r)}{| \bar{\mathbf{W}}(r) |} \begin{bmatrix} \frac{1}{2} \bar{\Omega}_R r \bar{W}_Y(r) & 0 & 0 & \frac{1}{2} r \{ \bar{W}_Y(r) \}^2 & 0 & \frac{1}{2} \bar{\Omega}_R r \bar{W}_Y(r) d \\ 0 & -\bar{\Omega}_R r \bar{W}_Y(r) & 0 & 0 & \bar{\Omega}_R^2 r^3 & 0 \\ 0 & 0 & \frac{1}{2} \bar{\Omega}_R r \bar{W}_Y(r) & -\frac{1}{2} \bar{\Omega}_R r \bar{W}_Y(r) d & 0 & \frac{1}{2} r \{ \bar{W}_Y(r) \}^2 \\ -\frac{1}{2} \bar{\Omega}_R^2 r^3 & 0 & -\frac{1}{2} \bar{\Omega}_R r \bar{W}_Y(r) d & \left(-\frac{1}{2} \bar{\Omega}_R r \bar{W}_Y(r) \right) & 0 & 0 \\ 0 & -r \bar{W}_Y(r) & 0 & \left(-\frac{1}{2} \bar{\Omega}_R r \bar{W}_Y(r) \right) & 0 & 0 \\ \frac{1}{2} \bar{\Omega}_R r \bar{W}_Y(r) d & 0 & -\frac{1}{2} \bar{\Omega}_R^2 r^3 & 0 & \bar{\Omega}_R r^3 \bar{W}_Y(r) & \left(-\frac{1}{2} \bar{\Omega}_R r \bar{W}_Y(r) \right) \end{bmatrix} dr. \end{aligned} \quad (6.21)$$

The third part, related to the aerodynamic excitation corresponding to the drag forces acting on the rotor, is found to be:

$$\begin{aligned} \frac{\partial \mathbf{Q}_{R:D}(t)}{\partial \dot{\mathbf{v}}^1(t)} \Big|_S = & \frac{3}{2} \int_{r_0}^R \rho c(r) C_D(r) |\bar{\mathbf{W}}(r)| \begin{bmatrix} -\frac{1}{2} & 0 & 0 & 0 & 0 & -\frac{1}{2}d \\ 0 & -1 & 0 & 0 & 0 & 0 \\ 0 & 0 & -\frac{1}{2} & \frac{1}{2}d & 0 & 0 \\ 0 & 0 & \frac{1}{2}d & -\frac{1}{2}(r^2 + d^2) & 0 & 0 \\ 0 & 0 & 0 & 0 & -r^2 & 0 \\ -\frac{1}{2}d & 0 & 0 & 0 & 0 & 0 \end{bmatrix} dr \\ + \frac{3}{2} \int_{r_0}^R \frac{\rho c(r) C_D(r)}{|\bar{\mathbf{W}}(r)|} & \begin{bmatrix} -\frac{1}{2}\bar{\Omega}_R^2 r^2 & 0 & 0 & -\frac{1}{2}\bar{\Omega}_R r^2 \bar{W}_Y(r) & 0 & -\frac{1}{2}\bar{\Omega}_R^2 r^2 d \\ 0 & -\{\bar{W}_Y(r)\}^2 & 0 & 0 & \bar{\Omega}_R r^2 \bar{W}_Y(r) & 0 \\ 0 & 0 & -\frac{1}{2}\bar{\Omega}_R^2 r^2 & \frac{1}{2}\bar{\Omega}_R^2 r^2 d & 0 & -\frac{1}{2}\bar{\Omega}_R r^2 \bar{W}_Y(r) \\ -\bar{\Omega}_R r^2 \bar{W}_Y(r) & 0 & \frac{1}{2}\bar{\Omega}_R^2 r^2 d & \left(-\frac{1}{2}\bar{\Omega}_R^2 r^2 d^2\right) & 0 & 0 \\ 0 & 2\bar{\Omega}_R r^2 \bar{W}_Y(r) & 0 & 0 & -\bar{\Omega}_R^2 r^4 & 0 \\ -\frac{1}{2}\bar{\Omega}_R^2 r^2 d & 0 & -\bar{\Omega}_R r^2 \bar{W}_Y(r) & 0 & 0 & \left(-\frac{1}{2}r^2 \{\bar{W}_Y(r)\}^2\right) \end{bmatrix} dr. \end{aligned} \quad (6.22)$$

The last of the four components, related to the inertia, is presented in Equation 6.23:

$$\frac{\partial \mathbf{Q}_{R:I}(t)}{\partial \dot{\mathbf{v}}^1(t)} \Big|_S = \frac{3}{2} \int_{r_0}^R \rho \pi c(r)^2 \begin{bmatrix} 0 & 0 & 0 & \bar{W}_Y(r) \bar{\Omega}_R & 0 & 0 \\ 0 & 0 & 0 & 0 & 0 & 0 \\ 0 & 0 & 0 & 0 & 0 & \bar{W}_Y(r) \bar{\Omega}_R \\ 0 & 0 & 0 & 0 & 0 & -\bar{W}_Y(r) \bar{\Omega}_R d \\ 0 & 0 & 0 & 0 & 0 & 0 \\ 0 & 0 & 0 & \bar{W}_Y(r) \bar{\Omega}_R d & 0 & 0 \end{bmatrix} dr. \quad (6.23)$$

6.2.4 AERODYNAMIC EXCITATION SENSITIVITY TO STRUCTURAL ACCELERATION

The sensitivity of the aerodynamic excitation to the structural accelerations of the tower top only consist of the partial derivative of the inertia component of the force:

$$\frac{\partial \mathbf{Q}_{R:A}(t)}{\partial \ddot{\mathbf{v}}^1(t)} \Big|_S = \frac{\partial \mathbf{Q}_{R:I}(t)}{\partial \dot{\mathbf{v}}^1(t)} \Big|_S, \quad (6.24)$$

where this sensitivity is defined as follows:

$$\frac{\partial \mathbf{Q}_{R:I}(t)}{\partial \ddot{\mathbf{v}}^1(t)} \Big|_S = \frac{3}{2} \int_{r_0}^R \rho \pi c(r)^2 \begin{bmatrix} 0 & 0 & 0 & -\bar{\Omega}_R d & 0 & \bar{W}_Y(r) \\ 0 & 0 & 0 & 0 & 0 & 0 \\ -\bar{\Omega}_R & 0 & 0 & -\bar{W}_Y(r) & 0 & -\bar{\Omega}_R d \\ \bar{\Omega}_R d & 0 & 0 & \bar{W}_Y(r) d & 0 & \bar{\Omega}_R (r^2 + d^2) \\ 0 & 0 & 0 & 0 & 0 & 0 \\ 0 & 0 & \bar{\Omega}_R d & -\bar{\Omega}_R (r^2 + d^2) & 0 & \bar{W}_Y(r) d \end{bmatrix} dr. \quad (6.25)$$

6.2.5 AERODYNAMIC EXCITATION SENSITIVITY TO ROTATIONAL VELOCITY VARIATIONS

This section describes the sensitivity of the aerodynamic excitation with respect to changes in the rotational velocity, which consist of the following three components:

$$\frac{\partial \mathbf{Q}_{R:A}(t)}{\partial \Omega_R(t)} \Big|_S = \frac{\partial \mathbf{Q}_{R:L}^a(t)}{\partial \Omega_R(t)} \Big|_S + \frac{\partial \mathbf{Q}_{R:L}^c(t)}{\partial \Omega_R(t)} \Big|_S + \frac{\partial \mathbf{Q}_{R:D}(t)}{\partial \Omega_R(t)} \Big|_S, \quad (6.26)$$

where the first of these components is defined as follows:

$$\begin{aligned} \left. \frac{\partial \mathbf{Q}_{R:L}^\alpha(t)}{\partial \Omega_R(t)} \right|_S &= \frac{3}{2} \int_{r_0}^R \rho c(r) C_L^\alpha(r) \sin(\beta_0(r) + \bar{\beta}) [0 \quad -2\bar{\Omega}_R r^2 \quad 0 \quad 0 \quad -r^2 \bar{W}_Y(r) \quad 0]^T dr \\ &+ \frac{3}{2} \int_{r_0}^R \rho c(r) C_L^\alpha(r) \cos(\beta_0(r) + \bar{\beta}) [0 \quad r \bar{W}_Y(r) \quad 0 \quad 0 \quad 0 \quad 0]^T dr. \end{aligned} \quad (6.27)$$

The sensitivity related to the component of the excitation corresponding the lift generated by the cambered shape of the airfoils is:

$$\begin{aligned} \left. \frac{\partial \mathbf{Q}_{R:L}^c(t)}{\partial \Omega_R(t)} \right|_S &= \frac{3}{2} \int_{r_0}^R \rho c(r) C_L^c(r) |\bar{\mathbf{W}}(r)| [0 \quad r \quad 0 \quad 0 \quad 0 \quad 0]^T dr \\ &+ \frac{3}{2} \int_{r_0}^R \frac{\rho c(r) C_L^c(r) \bar{\Omega}_R r^2}{|\bar{\mathbf{W}}(r)|} [0 \quad \bar{\Omega}_R r \quad 0 \quad 0 \quad r \bar{W}_Y(r) \quad 0]^T dr, \end{aligned} \quad (6.28)$$

and the drag related sensitivity is found to be:

$$\begin{aligned} \left. \frac{\partial \mathbf{Q}_{R:D}(t)}{\partial \Omega_R(t)} \right|_S &= \frac{3}{2} \int_{r_0}^R \rho c(r) C_D(r, W_Y) |\bar{\mathbf{W}}(r)| [0 \quad 0 \quad 0 \quad 0 \quad -r^2 \quad 0]^T dr \\ &+ \frac{3}{2} \int_{r_0}^R \frac{\rho c(r) C_D(r) \bar{\Omega}_R r^2}{|\bar{\mathbf{W}}(r)|} [0 \quad \bar{W}_Y(r) \quad 0 \quad 0 \quad -\bar{\Omega}_R r^2 \quad 0]^T dr. \end{aligned} \quad (6.29)$$

6.2.6 AERODYNAMIC EXCITATION SENSITIVITY TO PITCH ANGLE VARIATIONS

The only part of the aerodynamic excitation dependent on the pitch angle of the blades is the part of the excitation dependent on the angle of attack:

$$\left. \frac{\partial \mathbf{Q}_{R:A}(t)}{\partial \beta(t)} \right|_S = \left. \frac{\partial \mathbf{Q}_{R:L}^\alpha(t)}{\partial \beta(t)} \right|_S. \quad (6.30)$$

This sensitivity is presented in Equation 6.31:

$$\begin{aligned} \left. \frac{\partial \mathbf{Q}_{R:L}^\alpha(t)}{\partial \beta(t)} \right|_S &= \frac{3}{2} \int_{r_0}^R \rho c(r) C_L^\alpha(r) \cos(\beta_0(r) + \bar{\beta}) [0 \quad -\bar{\Omega}_R^2 r^2 \quad 0 \quad 0 \quad -\bar{\Omega}_R r^2 \bar{W}_Y(r) \quad 0]^T dr \\ &- \frac{3}{2} \int_{r_0}^R \rho c(r) C_L^\alpha(r) \sin(\beta_0(r) + \bar{\beta}) [0 \quad \bar{\Omega}_R r \bar{W}_Y(r) \quad 0 \quad 0 \quad \{\bar{W}_Y(r)\}^2 r \quad 0]^T dr. \end{aligned} \quad (6.31)$$

6.2.7 AERODYNAMIC EXCITATION SENSITIVITY TO INDUCTION FACTOR VARIATIONS

The final sensitivity that is presented, is the sensitivity of the aerodynamic excitation with respect to the induction factor, which is defined as:

$$\left. \frac{\partial \mathbf{Q}_{R:A}(t)}{\partial a(r, t)} \right|_S = \left. \frac{\partial \mathbf{Q}_{R:L}^\alpha(t)}{\partial a(r, t)} \right|_S + \left. \frac{\partial \mathbf{Q}_{R:L}^c(t)}{\partial a(r, t)} \right|_S + \left. \frac{\partial \mathbf{Q}_{R:D}(t)}{\partial a(r, t)} \right|_S. \quad (6.32)$$

The sensitivity is the sum of the partial derivatives of the excitation components with respect to the induction factor. The sensitivity related to the angle of attack dependent lift component is:

$$\begin{aligned} \left. \frac{\partial \mathbf{Q}_{R:L}^{\alpha}(t)}{\partial a(r, t)} \right|_S &= \frac{3}{2} \int_{r_0}^R \rho c(r) C_L^{\alpha}(r) \sin(\beta_0(r) + \bar{\beta}) [0 \ 0 \ 0 \ 0 \ \bar{\Omega}_R r^2 \bar{W}_{\infty} \ 0]^T dr \\ &+ \frac{3}{2} \int_{r_0}^R \rho c(r) C_L^{\alpha}(r) \cos(\beta_0(r) + \bar{\beta}) [0 \ -\bar{\Omega}_R r \bar{W}_{\infty} \ 0 \ 0 \ r \bar{W}_{\infty}^2 (2a(r) - 2) \ 0]^T dr, \end{aligned} \quad (6.33)$$

while the sensitivity related to the cambered shape of the airfoils is:

$$\begin{aligned} \left. \frac{\partial \mathbf{Q}_{R:L}^c(t)}{\partial a(r, t)} \right|_S &= \frac{3}{2} \int_{r_0}^R \rho c(r) C_L^c(r) |\bar{\mathbf{W}}(r)| [0 \ 0 \ 0 \ 0 \ -r \bar{W}_{\infty} \ 0]^T dr \\ &+ \frac{3}{2} \int_{r_0}^R \frac{\rho c(r) C_L^c(r)}{|\bar{\mathbf{W}}(r)|} [0 \ r \bar{\Omega}_R \bar{W}_{\infty}^2 (a(r) - 1) \ 0 \ 0 \ r \bar{W}_{\infty}^2 \bar{W}_Y(r) (a(r) - 1) \ 0]^T dr. \end{aligned} \quad (6.34)$$

Concluding, the drag related component of the sensitivity of the aerodynamic excitation to changes in the induction factor is found to be as follows:

$$\begin{aligned} \left. \frac{\partial \mathbf{Q}_{R:D}(t)}{\partial a(r, t)} \right|_S &= \frac{3}{2} \int_{r_0}^R \rho c(r) C_D(r) |\bar{\mathbf{W}}(r)| [0 \ -\bar{W}_{\infty} \ 0 \ 0 \ 0 \ 0]^T dr \\ &+ \frac{3}{2} \int_{r_0}^R \frac{\rho c(r) C_D(r)}{|\bar{\mathbf{W}}(r)|} [0 \ \bar{W}_{\infty}^2 \bar{W}_Y(r) (a(r) - 1) \ 0 \ 0 \ \bar{\Omega}_R r^2 \bar{W}_{\infty}^2 (a(r) - 1) \ 0]^T dr. \end{aligned} \quad (6.35)$$

6.3 NUMERICAL MODEL

The following set of differential equations describes the model with linearized aerodynamic excitation, and is solved in Matlab. As in the previous chapter, modal analysis is applied.

$$\left\{ \begin{array}{l} \ddot{\mathbf{w}}(t) = A^{-1} B \\ \Delta \dot{\Omega}_R(t) = T_{R:A,Y}(t) - C_{DT} \left(\Delta \Omega_R(t) - \frac{1}{N_{GB}} \Delta \Omega_G(t) \right) - K_{DT} \left(\int_0^t \Delta \Omega_R(t) dt - \frac{1}{N_{GB}} \int_0^t \Delta \Omega_G(t) dt \right) \\ \Delta \dot{\Omega}_G(t) = -T_G - C_{DT} \left(\frac{1}{N_{GB}^2} \Delta \Omega_G(t) - \frac{1}{N_{GB}} \Delta \Omega_R(t) \right) - K_{DT} \left(\frac{1}{N_{GB}^2} \int_0^t \Delta \Omega_G(t) dt - \frac{1}{N_{GB}} \int_0^t \Delta \Omega_R(t) dt \right) \\ \Delta \dot{\beta}(t) = K_P \left(-T_G - C_{DT} \left(\frac{1}{N_{GB}^2} \Delta \Omega_G(t) - \frac{1}{N_{GB}} \Delta \Omega_R(t) \right) - K_{DT} \left(\frac{1}{N_{GB}^2} \int_0^t \Delta \Omega_G(t) dt - \frac{1}{N_{GB}} \int_0^t \Delta \Omega_R(t) dt \right) \right) \\ \dot{\mathbf{a}}(t) = \text{Equation 2.16} \end{array} \right\}$$

Where the matrices A and B are defined as follows:

$$A = \mathbf{E}^T \left[\mathbf{M} + \begin{bmatrix} \left. \frac{\partial \mathbf{Q}_{R:A}(t)}{\partial \dot{\mathbf{v}}^T(t)} \right|_S & \mathbf{0}_{6 \times (n-6)} \\ \mathbf{0}_{(n-6) \times 6} & \mathbf{0}_{(n-6) \times (n-6)} \end{bmatrix} \right] \mathbf{E}, \quad (6.36)$$

and:

$$\begin{aligned}
B = & \mathbf{E}^T \begin{bmatrix} \bar{\mathbf{Q}}_{R:A} \Big|_S \\ \mathbf{0}_{(n-6) \times 1} \end{bmatrix} + \mathbf{E}^T \begin{bmatrix} \frac{\partial \mathbf{Q}_{R:A}(t)}{\partial W_Y(t)} \Big|_S \Delta W_Y(t) \\ \mathbf{0}_{(n-6) \times 1} \end{bmatrix} + \mathbf{E}^T \begin{bmatrix} \frac{\partial \mathbf{Q}_{R:A}(t)}{\partial \Omega_R(t)} \Big|_S \Delta \Omega_R(t) \\ \mathbf{0}_{(n-6) \times 1} \end{bmatrix} + \mathbf{E}^T \begin{bmatrix} \frac{\partial \mathbf{Q}_{R:A}(t)}{\partial \beta(t)} \Big|_S \Delta \beta(t) \\ \mathbf{0}_{(n-6) \times 1} \end{bmatrix} \\
& + \mathbf{E}^T \begin{bmatrix} \frac{\partial \mathbf{Q}_{R:A}(t)}{\partial a(t)} \Big|_S \Delta a(t) \\ \mathbf{0}_{(n-6) \times 1} \end{bmatrix} + \mathbf{E}^T \begin{bmatrix} \frac{\partial \mathbf{Q}_{R:A}(t)}{\partial \dot{\mathbf{v}}^1(t)} \Big|_S & \mathbf{0}_{6 \times (n-6)} \\ \mathbf{0}_{(n-6) \times 6} & \mathbf{0}_{(n-6) \times (n-6)} \end{bmatrix} \mathbf{E} \dot{\mathbf{w}}(t) + \mathbf{E}^T \begin{bmatrix} \frac{\partial \mathbf{Q}_{R:A}(t)}{\partial \mathbf{v}^1(t)} \Big|_S & \mathbf{0}_{6 \times (n-6)} \\ \mathbf{0}_{(n-6) \times 6} & \mathbf{0}_{(n-6) \times (n-6)} \end{bmatrix} \mathbf{E} \mathbf{w}(t) \\
& - \mathbf{E}^T \begin{bmatrix} \mathbf{0}_{4 \times 1} \\ I_R \Delta \dot{\Omega}_R(t) + I_G \Delta \dot{\Omega}_G(t) \\ \mathbf{0}_{(n-5) \times 1} \end{bmatrix} - \mathbf{E}^T \mathbf{C} \mathbf{E} \dot{\mathbf{w}}(t) - \mathbf{E}^T \mathbf{K} \mathbf{E} \mathbf{w}(t).
\end{aligned} \tag{6.37}$$

The aerodynamic torque $T_{R:A;Y}(t)$ is approximated as:

$$\begin{aligned}
T_{R:A;Y}(t) = & \bar{T}_{R:A;Y} \Big|_S + \frac{\partial T_{R:A;Y}(t)}{\partial W_Y(r, t)} \Big|_S \Delta W_Y(r, t) + \frac{\partial T_{R:A;Y}(t)}{\partial \Omega_R(t)} \Big|_S \Delta \Omega_R(t) + \frac{\partial T_{R:A;Y}(t)}{\partial \beta(t)} \Big|_S \Delta \beta(t) \\
& + \frac{\partial T_{R:A;Y}(t)}{\partial a(r, t)} \Big|_S \Delta a(r, t) + \frac{\partial T_{R:A;Y}(t)}{\partial \dot{\mathbf{v}}^1(t)} \Big|_S \mathbf{E}^1 \dot{\mathbf{w}}(t) + \frac{\partial T_{R:A;Y}(t)}{\partial \mathbf{v}^1(t)} \Big|_S \mathbf{E}^1 \mathbf{w}(t) \\
& + \frac{\partial T_{R:A;Y}(t)}{\partial \mathbf{v}^1(t)} \Big|_S \mathbf{E}^1 \mathbf{w}(t),
\end{aligned} \tag{6.38}$$

where \mathbf{E}^1 contains the modal amplitudes of the degrees of freedom corresponding to the tower top, or node 1.

6.4 COMPARISON

The model presented in Chapter 5 and the model described in this chapter are compared in this section. The same turbulent input as used in previous chapters is used, see Figure 6.1.a, and only the first two mode shapes are taken into account. As expected from the results obtained in Chapter 4, the sensitivity of the aerodynamic torque to the pitch angle is underestimated in the linearized aerodynamic torque. This underestimation results in a pitch angle which is higher than the pitch angle of the model using the nonlinear aerodynamic excitation, as Figure 6.1.c shows. The largest differences occur for wind velocities that are the furthest away from the operational state S , chosen to be at a wind velocity of 15 m/s. The lower sensitivity of the aerodynamic torque to changes in pitch angle results in larger deviations of the rotational velocity of the rotor from its rated value (Figure 6.1), due to the rotational velocity reacting slower to the changes in pitch angle. The linearized aerodynamic torque and thrust approximate the nonlinear ones very well, as can be seen in Figure 6.1.d and 6.1.e, respectively. The more fluctuating pitch angle of the linearized excitation model results in a more fluctuating thrust force, this in turn leads to a slightly larger amplitude of the fore-aft motion of the tower top, as is presented in Figure 6.2.b. The side-to-side motion (Figure 6.2.a) matches well, and the frequency spectra corresponding to the side-to-side and fore-aft motions of the tower top have peaks at the same frequencies.

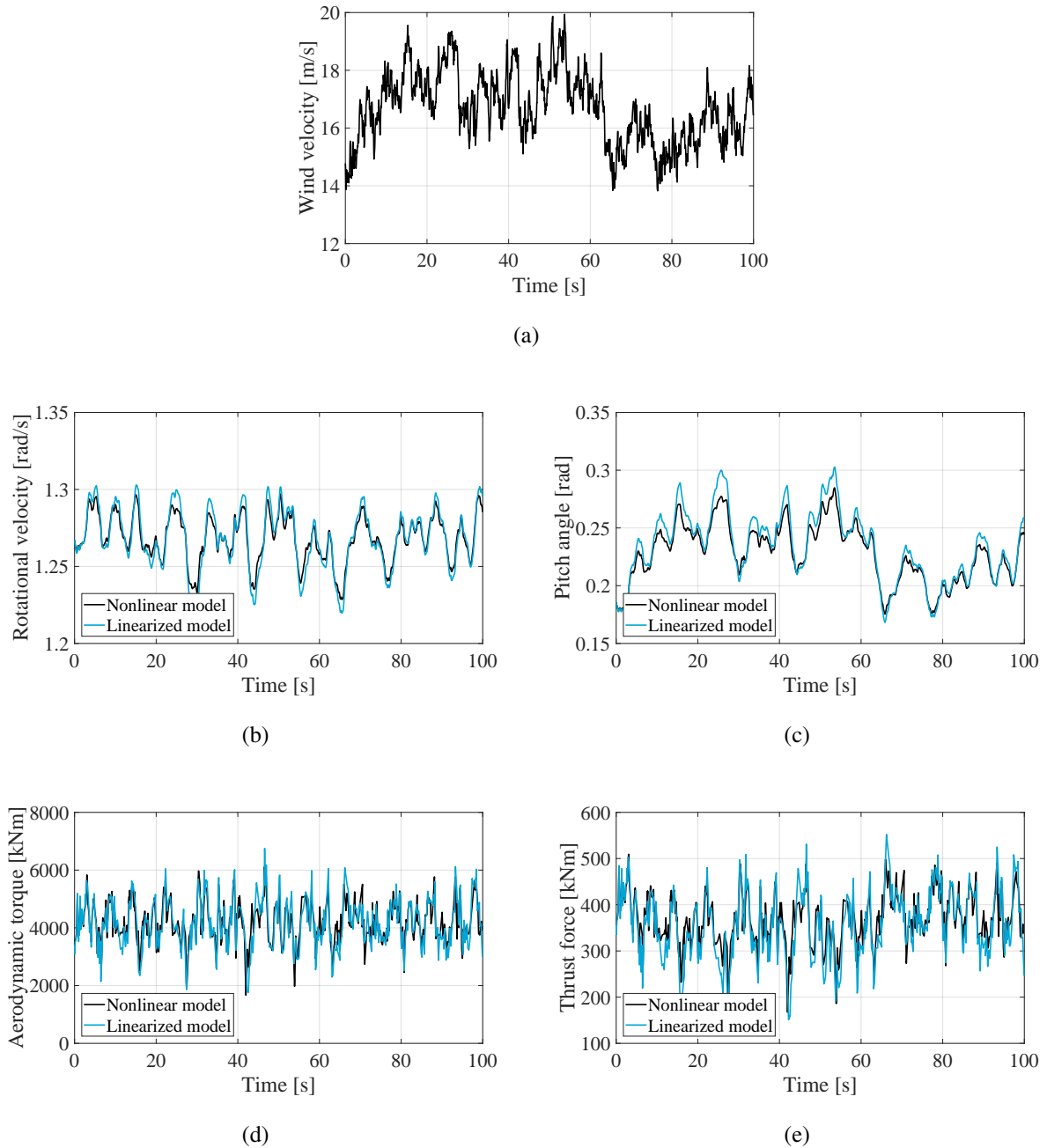


Figure 6.1: Results for turbulent wind input with wind signal (a), rotational velocity (b), pitch angle (c), aerodynamic torque (d) and thrust force (e) for both nonlinear and linearized aerodynamic excitation.

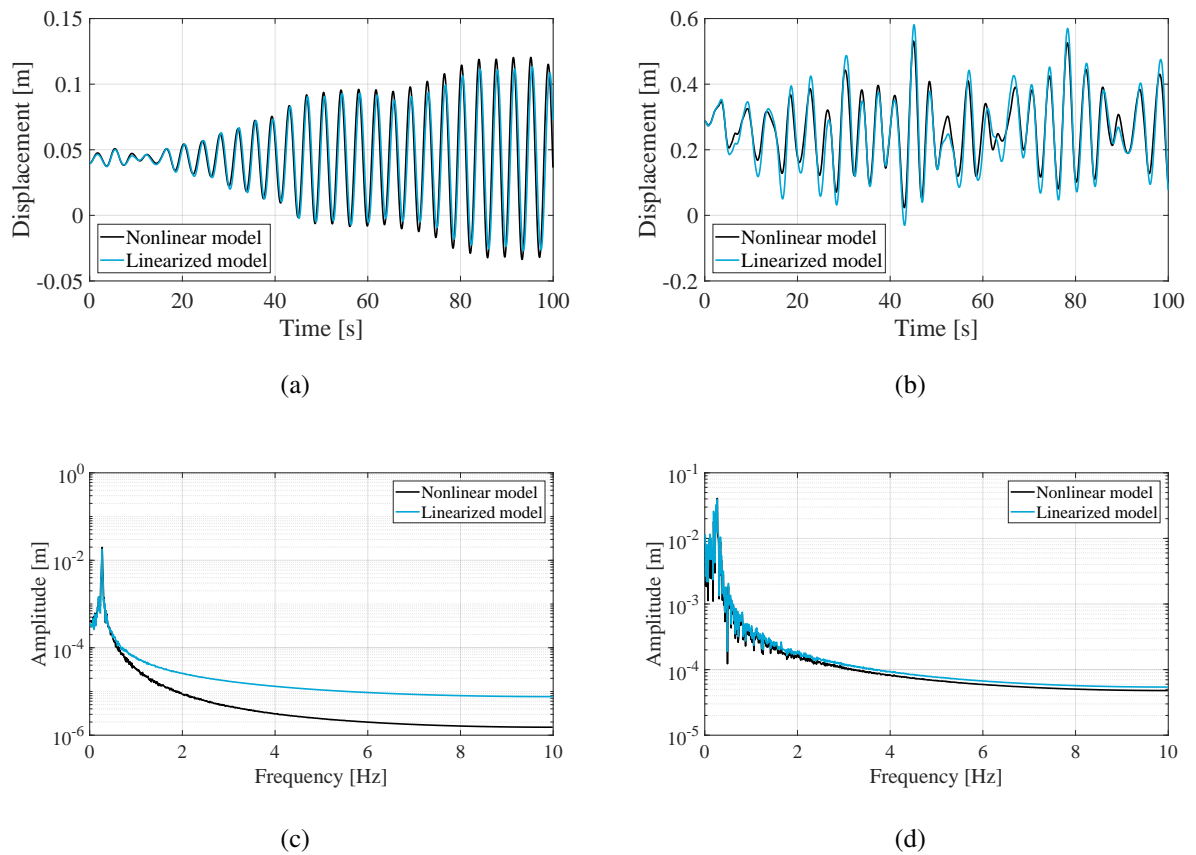


Figure 6.2: Side-to-side displacement of the tower top $u_x^1(t)$ (a), fore-aft motion of the tower top $u_y^1(t)$ (b), the side-to-side motion in the frequency domain (c) and the fore-aft displacement in the frequency domain (d).

7 | CONCLUSIONS AND RECOMMENDATIONS

When comparing the full model including a flexible drivetrain shaft and tower structure using the nonlinear aerodynamic excitation model with Bladed some differences in excitation and motions are observed. The difference in thrust force is largely explained by the difference in pitch angles. While in the time domain, some differences in amplitude are seen, when the tower top motions in X and Y direction are analyzed in the frequency domain, it is seen they behave similarly, except for some difference in the height of the peaks. Some differences between the model and Bladed are inevitable, since time independent lift and drag coefficients are used, and Chapter 3 shows that the low angle of attack assumption is not always valid. The initial conditions of the displacement of the support structure are different, which hints at either differences in the support structure model, or a different definition of the initial conditions. Finally, Bladed is found to converge to slightly different pitch angles to obtain equilibrium, this difference will influence the behavior of all other parameters, thus a true match cannot be expected and the results found are sufficient enough to validate the model, concluding that it is possible to create a model which approaches software simulation tools in accuracy, while increasing insight and reducing computational expense. Although no in depth study into the differences between computational time is done, the unoptimized code has shown to be at least fifty times faster than Bladed. For the computational expense to be reduced as much as possible, the code should be optimized.

The linearization of the aerodynamic excitation with respect to the wind velocity, structural motions, rotational rotor velocity, pitch angle and induction factor is a reasonable approximation of the nonlinear excitation. However, it is important to note that the accuracy decreases with the wind velocity being further away from the chosen mean operating point. The applicability of the linearized aerodynamic excitation is therefore dependent on the degree of turbulence present in the wind and the desired accuracy. The turbulent signal used is a relatively high-turbulence signal, and even with this signal acceptable results are obtained, logically, the approximation will be better for wind signals with a lower turbulence intensity. More research is needed to quantify the region for which valid results are obtained with the model using linearized excitation and what the limits of its applicability are. The accuracy of the approximation could be improved by increasing the order of the Taylor series expansion used to capture the nonlinear nature of the aerodynamic excitation, however, this will result in a more terms and a second order dependency. Evaluating the lift and drag coefficients at the mean operating points and keeping them constant has a negligible effect on the results, while the use of different wake models is shown to have significant effect.

Since the model is based on several fundamental assumptions, there is room for improvement of the model presented in this thesis, although each of these improvements will result in a more realistic model, it will also increase its complexity. The model can be improved by allowing the wind velocity to not be unidirectional but have an angle with respect to the drivetrain axis and be non uniform to have a more realistic wind description. By allowing the blades to be different, the model would be more realistic (and more complex) and could describe a situation in which for example one blade is covered by ice, resulting in a different mass and shape. The blades can also be assigned degrees of freedom, allowing them to bend, losing the assumption of rigidity. In this thesis, only the above rated regime is considered, where the pitch angle controller is active. If the below rated

regime would be included in the model as well, for that regime an active generator torque controller should be implemented, making the model usable for every operational wind condition. Possible extensions of the model are the addition of hydrodynamic or ice loads, or using a different type of support structure, such as a jacket, floating platform or spar.

BIBLIOGRAPHY

- [1] E.A. Bossanyi. *GH Bladed Theory Manual*. Garrad Hassan and Partners Limited, September 2010.
- [2] Tony Burton, David Sharpe, Nick Jenkins, and Ervin Bossanyi. *Wind Energy Handbook*. John Wiley & Sons Ltd, 2001.
- [3] T. Fischer, W. de Vries, and B. Schmidt. Upwind design basis (wp4: Offshore foundations and support structures). *Project UpWind*, October 2010.
- [4] Morten H. Hansen, Anca Hansen, Torben J. Larsen, Stig Oye, Poul Sorensen, and Peter Fuglsang. Control design for a pitch-regulated, variable speed wind turbine. *Riso National Laboratory, Roskilde*, January 2005.
- [5] Andrew Ho and Ariola Mbistrova. The european offshore wind industry, key trends and statistics 2016. *WindEurope*, January 2017.
- [6] Abdulhamed Hwas and Reza Katebi. Wind turbine control using pi pitch angle controller. *Industrial Control Centre, University of Strathclyde, Glasgow*, March 2012.
- [7] J. Jonkman, S. Butterfield, W. Musial, and G. Scott. Definition of a 5-mw reference wind turbine for offshore system development. *National Renewable Energy Laboratory*, February 2009.
- [8] J. Jonkman and W. Musial. Offshore code comparison collaboration (oc3) for iea task 23 offshore wind technology and development. *National Renewable Energy Laboratory*, December 2010.
- [9] S.M. Muyeen, Junji Tamura, and Toshiaki Murata. *Stability Augmentation of a Grid-connected Wind Farm*. Springer, 2008.
- [10] Pim van der Male, Karel N. van Dalen, and Andrei V. Metrikine. Definition of the coupling between the aerodynamic force on a wind turbine rotor and the tower top motions through force-response interaction matrices. *Department of Hydraulic Engineering, Delft University of Technology and Department of Structural Engineering, Delft University of Technology*, 2017.
- [11] Zili Zhang, Soren R. K. Nielsen, Frede Blaabjerg, and Dao Zhou. Dynamics and control of lateral tower vibrations in offshore wind turbines by means of active generator torque. *Energies*, November 2014.

A | NREL 5-MW REFERENCE WIND TURBINE

This appendix contains specifications and operational parameters of the NREL 5-MW Reference Wind Turbine.

A.1 BLADE PROPERTIES

The blades are divided in eighteen sections of which various parameters are specified in Table A.1. The specifications are evaluated at the center of the sections.

Section number	Mass [kg]	Length [m]	Chord length [m]	Distance from hub [m]	Structural twist [rad]
1	760.02	1.369	3.521	2.034	0.2323
2	720.26	2.751	3.698	4.094	0.2323
3	531.85	2.740	4.011	6.840	0.2323
4	436.55	3.456	4.362	9.937	0.2323
5	405.98	4.140	4.605	13.734	0.2163
6	360.86	4.104	4.555	17.857	0.1889
7	344.56	4.103	4.354	21.960	0.1673
8	321.16	4.105	4.128	26.064	0.1467
9	289.89	4.101	3.878	30.167	0.1251
10	259.56	4.100	3.625	34.267	0.1039
11	223.94	4.100	3.379	38.368	0.0833
12	185.05	4.109	3.133	42.473	0.0638
13	154.67	4.101	2.887	46.578	0.0475
14	124.44	4.100	2.641	50.679	0.0336
15	99.47	3.417	2.416	54.437	0.0208
16	81.11	2.739	2.200	57.515	0.0108
17	59.80	2.737	1.753	60.253	0.0042
18	29.68	1.368	0.810	62.308	0.0009

Table A.1: The blade specifications [7].

A.2 LIFT AND DRAG COEFFICIENTS

The coefficients of each section in the above rated regime are presented in Table A.2, Table A.3 and Table A.4.

Section	C_L^c
1	0.0000
2	0.0000
3	0.0000
4	0.0685
5	0.1665
6	0.1960
7	0.2420
8	0.3660
9	0.4440
10	0.4825
11	0.5210
12	0.4815
13	0.4420
14	0.4420
15	0.4420
16	0.4420
17	0.4420
18	0.4420

Table A.2: The cambered lift coefficients C_L^c of the sections [7].

Section	11 m/s	12 m/s	13 m/s	14 m/s	15 m/s	16 m/s	17 m/s	18 m/s	19 m/s	20 m/s	21 m/s	22 m/s	23 m/s	24 m/s	25 m/s
1	0.0000	0.0000	0.0000	0.0000	0.0000	0.0000	0.0000	0.0000	0.0000	0.0000	0.0000	0.0000	0.0000	0.0000	0.0000
2	0.0000	0.0000	0.0000	0.0000	0.0000	0.0000	0.0000	0.0000	0.0000	0.0000	0.0000	0.0000	0.0000	0.0000	0.0000
3	0.0000	0.0000	0.0000	0.0000	0.0000	0.0000	0.0000	0.0000	0.0000	0.0000	0.0000	0.0000	0.0000	0.0000	0.0000
4	0.0000	1.8196	1.8218	1.8193	1.8172	1.8160	1.8075	1.8021	1.7977	1.7948	1.7932	1.7935	1.7958	1.7992	1.8036
5	0.0000	5.9821	5.8677	5.7471	5.6406	5.5490	5.4540	5.3696	5.2958	5.2327	5.1730	5.1237	5.0800	5.0433	5.0131
6	0.0000	7.0017	6.9192	6.8292	6.7492	6.6755	6.6067	6.5358	6.4721	6.4151	6.3540	6.2998	6.2469	6.1970	6.1538
7	0.0000	7.1910	7.1407	7.0898	7.0395	6.9904	6.9427	6.8980	6.8577	6.8212	6.7852	6.7512	6.7193	6.6850	6.6534
8	0.0000	7.0803	7.0334	6.9895	6.9421	6.8980	6.8574	6.8195	6.7846	6.7538	6.7249	6.6975	6.6718	6.6452	6.6199
9	0.0000	6.9999	6.9376	6.8647	6.7912	6.7307	6.6745	6.6240	6.5772	6.5358	6.4967	6.4597	6.4277	6.3964	6.3679
10	0.0000	6.9619	6.8858	6.7884	6.6582	6.5123	6.3299	6.0990	5.8109	5.4739	5.0382	4.4702	3.8745	3.2446	2.6057
11	0.0000	6.8484	6.7435	6.5938	6.2292	4.9563	19.1425	9.0059	8.2554	7.9748	7.8278	7.7347	7.6741	7.6335	7.6046
12	0.0000	6.6252	6.5526	6.4102	5.8673	9.3714	7.3727	7.1200	7.0248	6.9738	6.9441	6.9314	6.9463	6.9570	6.9650
13	0.0000	6.4395	6.3876	6.2624	5.1328	6.9231	6.6890	6.6295	6.6064	6.6168	6.6435	6.6684	6.6957	6.6739	6.6560
14	0.0000	6.4614	6.4223	6.2902	7.9258	6.6781	6.6038	6.5847	6.6047	6.6579	6.7107	6.6898	1.8482	-12.3642	6.6093
15	0.0000	6.4695	6.4357	6.2907	7.2435	6.6560	6.6056	6.5898	6.6598	6.7262	6.7243	2.1144	2.1023	-24.2570	6.6614
16	0.0000	6.4771	6.4446	6.3200	7.1972	6.6462	6.6050	6.6007	6.6971	6.7558	6.6810	2.2878	6.6080	6.6849	6.7468
17	0.0000	6.4874	6.4612	6.3753	6.9825	6.6066	6.5866	6.6263	6.7240	6.7189	22.1565	6.6165	6.6891	6.7489	6.7664
18	0.0000	6.5096	6.4947	6.4538	6.9656	6.5806	6.5777	1.8208	3.9422	8.8200	17.9628	-23.0254	6.7730	6.7828	6.7623

Table A.3: The angle of attack dependent lift coefficients C_L^α of the sections for different wind velocities in the above rated regime [7].

Section	11 m/s	12 m/s	13 m/s	14 m/s	15 m/s	16 m/s	17 m/s	18 m/s	19 m/s	20 m/s	21 m/s	22 m/s	23 m/s	24 m/s	25 m/s
1	0.5000	0.5000	0.5000	0.5000	0.5000	0.5000	0.5000	0.5000	0.5000	0.5000	0.5000	0.5000	0.5000	0.5000	0.5000
2	0.5000	0.5000	0.5000	0.5000	0.5000	0.5000	0.5000	0.5000	0.5000	0.5000	0.5000	0.5000	0.5000	0.5000	0.5000
3	0.4250	0.4250	0.4250	0.4250	0.4250	0.4250	0.4250	0.4250	0.4250	0.4250	0.4250	0.4250	0.4250	0.4250	0.4250
4	0.2542	0.2369	0.2419	0.2504	0.2595	0.2688	0.2781	0.2859	0.2933	0.2997	0.3047	0.3085	0.3113	0.3132	0.3144
5	0.0862	0.0682	0.0733	0.0820	0.0914	0.1011	0.1109	0.1193	0.1274	0.1344	0.1402	0.1447	0.1483	0.1510	0.1528
6	0.0128	0.0119	0.0120	0.0122	0.0125	0.0130	0.0135	0.0142	0.0148	0.0155	0.0163	0.0172	0.0181	0.0189	0.0197
7	0.0109	0.0104	0.0103	0.0103	0.0104	0.0104	0.0105	0.0105	0.0106	0.0107	0.0107	0.0108	0.0109	0.0110	0.0111
8	0.0089	0.0083	0.0082	0.0082	0.0082	0.0082	0.0082	0.0082	0.0082	0.0082	0.0083	0.0083	0.0083	0.0083	0.0084
9	0.0076	0.0070	0.0069	0.0068	0.0068	0.0068	0.0067	0.0067	0.0067	0.0067	0.0067	0.0067	0.0067	0.0067	0.0067
10	0.0073	0.0065	0.0063	0.0063	0.0062	0.0062	0.0062	0.0062	0.0061	0.0061	0.0061	0.0061	0.0061	0.0061	0.0061
11	0.0072	0.0060	0.0058	0.0058	0.0057	0.0057	0.0057	0.0057	0.0057	0.0057	0.0057	0.0057	0.0057	0.0057	0.0057
12	0.0064	0.0056	0.0055	0.0055	0.0055	0.0055	0.0055	0.0055	0.0055	0.0055	0.0055	0.0056	0.0057	0.0058	0.0059
13	0.0057	0.0053	0.0052	0.0052	0.0052	0.0052	0.0052	0.0052	0.0053	0.0054	0.0056	0.0058	0.0060	0.0062	0.0064
14	0.0057	0.0053	0.0052	0.0052	0.0052	0.0052	0.0052	0.0053	0.0055	0.0058	0.0061	0.0064	0.0067	0.0069	0.0071
15	0.0061	0.0053	0.0052	0.0052	0.0052	0.0052	0.0053	0.0054	0.0057	0.0061	0.0065	0.0068	0.0071	0.0073	0.0075
16	0.0070	0.0053	0.0053	0.0052	0.0052	0.0052	0.0053	0.0054	0.0059	0.0063	0.0067	0.0070	0.0073	0.0075	0.0078
17	0.0087	0.0053	0.0053	0.0052	0.0052	0.0052	0.0053	0.0056	0.0061	0.0065	0.0069	0.0073	0.0075	0.0078	0.0080
18	0.0109	0.0054	0.0053	0.0052	0.0052	0.0052	0.0053	0.0057	0.0063	0.0067	0.0071	0.0075	0.0078	0.0080	0.0081

Table A.4: The drag coefficients (C_D) of the sections for different wind velocities in the above rated regime [7].

Wind velocity [m/s]	Pitch angle [rad]
11	0.0000
12	0.0784
13	0.1212
14	0.1556
15	0.1857
16	0.2131
17	0.2385
18	0.2625
19	0.2851
20	0.3068
21	0.3279
22	0.3484
23	0.3680
24	0.3871
25	0.4055

Table A.5: Equilibrium pitch angles for different wind velocities in the above rated regime provided by Bladed.